

Performance of the CMS cathode strip chambers with cosmic rays

To cite this article: CMS Collaboration 2010 *JINST* 5 T03018

View the [article online](#) for updates and enhancements.

Related content

- [Performance of the CMS drift-tube chamber local trigger with cosmic rays](#)
CMS Collaboration
- [Performance study of the CMS barrel resistive plate chambers with cosmic rays](#)
CMS Collaboration
- [Performance of CMS hadron calorimeter timing and synchronization using test beam, cosmic ray, and LHC beam data](#)
CMS Collaboration

Recent citations

- [The performance of the CMS muon detector in proton-proton collisions at \$s = 7\$ TeV at the LHC](#)
The CMS collaboration
- [CMS muon detector and trigger performance](#)
Davide Piccolo
- [Performance of CMS muon reconstruction in cosmic-ray events](#)
CMS Collaboration

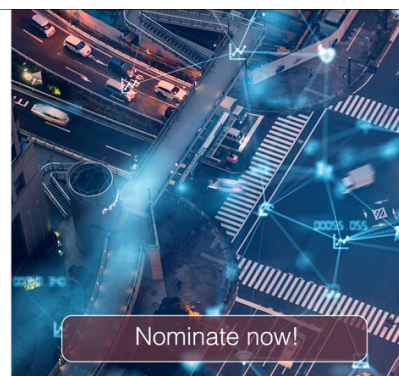


The Electrochemical Society
Advancing solid state & electrochemical science & technology

The ECS is seeking candidates to serve as the **Founding Editor-in-Chief (EIC) of ECS Sensors Plus**, a journal in the process of being launched in 2021

The goal of ECS Sensors Plus, as a one-stop shop journal for sensors, is to advance the fundamental science and understanding of sensors and detection technologies for efficient monitoring and control of industrial processes and the environment, and improving quality of life and human health.

Nomination submission begins: May 18, 2021



COMMISSIONING OF THE CMS EXPERIMENT WITH COSMIC RAYS

Performance of the CMS cathode strip chambers with cosmic rays

CMS Collaboration

ABSTRACT: The Cathode Strip Chambers (CSCs) constitute the primary muon tracking device in the CMS endcaps. Their performance has been evaluated using data taken during a cosmic ray run in fall 2008. Measured noise levels are low, with the number of noisy channels well below 1%. Coordinate resolution was measured for all types of chambers, and fall in the range $47 \mu\text{m}$ to $243 \mu\text{m}$. The efficiencies for local charged track triggers, for hit and for segments reconstruction were measured, and are above 99%. The timing resolution per layer is approximately 5 ns.

KEYWORDS: Large detector systems for particle and astroparticle physics; Particle tracking detectors (Gaseous detectors)

ARXIV EPRINT: [0911.4992](https://arxiv.org/abs/0911.4992)

Contents

1	Introduction	1
2	The CSC system	2
3	Reconstruction of muon track segments	5
4	Basic information from cosmic rays	6
5	Noise	8
6	Efficiency	10
6.1	LCT efficiencies	11
6.2	Strip and wire group efficiencies	12
6.3	Rechit efficiency	12
6.4	Segment efficiency	13
6.5	Attachment efficiency	13
7	Resolution	13
7.1	Methodology	14
7.2	Results from CRAFT	17
7.3	Measurements of the resolution	19
7.4	Special studies for ME1/1	20
8	Timing	21
9	Summary	21
	The CMS collaboration	24

1 Introduction

The primary goal of the Compact Muon Solenoid (CMS) experiment [1] is to explore particle physics at the TeV energy scale, exploiting the proton-proton collisions delivered by the Large Hadron Collider (LHC) at CERN [2]. The central feature of the CMS apparatus is a superconducting solenoid, of 6 m internal diameter, providing a field of 3.8 T. Within the field volume are the silicon pixel and strip tracking detectors, the crystal electromagnetic calorimeter and the brass/scintillator hadron calorimeter. Muons are measured in gas-ionization detectors embedded in the steel return yolk. In addition to the barrel and endcap detectors, CMS has extensive forward calorimetry.

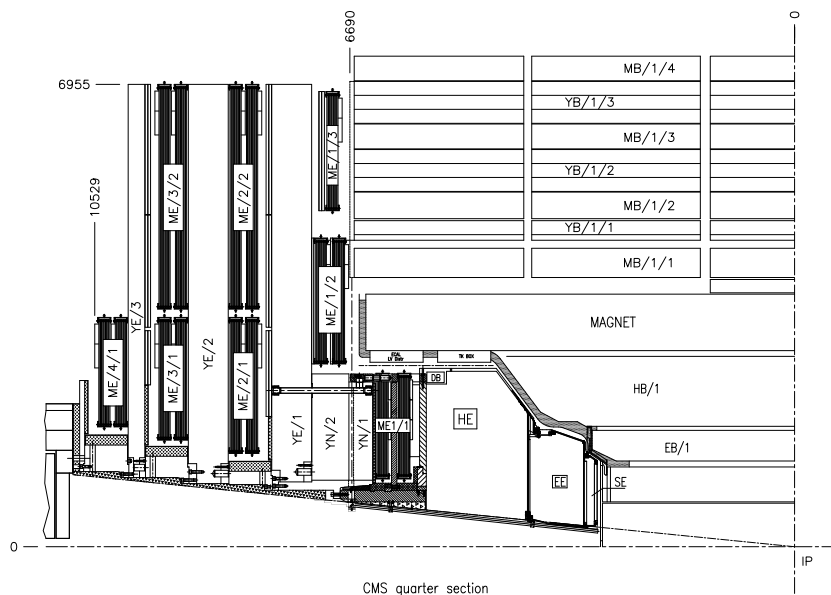


Figure 1. A cross-sectional view of a quarter of the CMS detector, highlighting the CSCs.

The Cathode Strip Chambers (CSCs) constitute an essential component of the CMS muon detector, providing precise tracking and triggering of muons in the endcaps. Their performance is critical to many physics analyses based on muons. An early assessment of their performance is possible using data recorded during the fall of 2008 as part of the Cosmic Run At Four Tesla (CRAFT) exercise. This paper summarizes the results obtained from the analysis of those data.

The CRAFT campaign involved all installed subdetector systems, most of which were nearly fully operational, as described in ref. [3]. Approximately 270 million cosmic ray muon triggers were recorded while the magnet was operating at a field of 3.8 T. Of these, roughly a fifth were triggered by the CSCs.

In the sections that follow, a selection of distributions characteristic of the flux of cosmic ray muons through the CSCs is shown, followed by an assessment of the electronics noise, measurements of the efficiency and resolution of the chambers, and finally some basic information about the timing capabilities of the CSCs. This paper begins with a brief description of the CSC muon system and of the basics of offline muon reconstruction.

2 The CSC system

The CSC subdetector is composed of rings of trapezoidal chambers mounted on eight disks - four in each endcap [4]. There are 468 chambers in total. The rings of chambers are designated by $ME_{\pm S/R}$, where “ME” stands for “Muon Endcap,” the \pm sign indicates which endcap, S indicates the disk (or “station”) and R is the ring number. The chambers in the outer rings, such as $ME_{\pm 2/2}$ and $ME_{\pm 3/2}$, are considerably larger than the chambers closer to the beam pipe, such as $ME_{\pm 1/1}$ and $ME_{\pm 1/2}$. A drawing of CMS highlighting the CSC subdetector is shown in figure 1.

Table 1. Selected physical specifications of the cathode strip chambers. The range of strip width is given, and the average width in square brackets. For more information, see ref. [4].

Ring	Chambers per ring	Strips per chamber	Strip width (mm)	Pitch (mrad)
ME±1/1 <i>a</i>	36	48	4.11 – 5.82 [4.96]	3.88
ME±1/1 <i>b</i>	36	64	4.44 – 7.6 [6.0]	2.96
ME±1/2	36	80	6.6 – 10.4 [8.5]	2.33
ME±1/3	36	64	11.1 – 14.9 [13.0]	2.16
ME±2/1	18	80	6.8 – 15.6 [11.2]	4.65
ME±2/2	36	80	8.5 – 16.0 [12.2]	2.33
ME±3/1	18	80	7.8 – 15.6 [11.7]	4.65
ME±3/2	36	80	8.5 – 16.0 [12.2]	2.33
ME±4/1	18	80	8.6 – 15.6 [12.1]	4.65

Every chamber contains six detecting layers each composed of an anode wire plane stretched between two planar copper cathodes, one continuous, the other segmented in strips to provide position measurement. The distance between anode planes is 2.54 cm, except for the ME±1/1 chambers, for which it is 2.2 cm. The wires are read out in groups, of which the width varies between 1.5 and 5 cm for different chambers. The high voltage is supplied to ranges of wire groups, depending on the size of the chamber; the largest chambers have five such high-voltage segments. The strips are read out individually, and their average widths vary between 5 and 12 mm. They are trapezoidal in shape, like the chambers themselves. The strips in alternating layers are staggered, except in ME±1/1. The strips in the ME±1/1 chambers are cut along a line parallel to the short sides of the trapezoid in order to reduce the rate on any one strip. The strips closer to the beam line constitute ME±1/1*a*, and the others, ME±1/1*b*. The studies presented in this paper concern ME±1/1*b* only. The smaller chambers tend to have a lower electronics noise due to smaller capacitive coupling between the wire and strip planes, better resolution due to smaller strip widths, and, in the case of ME±1/1, higher gas gain. A synopsis of relevant cathode strip parameters is given in table 1.

The CSCs are designed to measure the azimuthal coordinates (ϕ) of muon tracks well, as the bending of the muon trajectories in the magnetic flux returned through the steel disks is mainly about the direction of a unit vector pointing away from the beam line. The strips describe constant ϕ values. High precision is achieved by exploiting the shape of the charge distribution on three consecutive strips; this allows an adequate measurement of the muon momentum as needed for triggering purposes. The anode wires run perpendicular to the central strip, and hence parallel to the two parallel sides of the chamber; they provide an approximate measure of the radial coordinate. They are tilted by 29° in ME±1/1 to compensate for the average effect of the magnetic field on the drift. In terms of the local coordinate system, defined at the level of a single chamber, the six layers are parallel to the xy plane, with the y axis perpendicular to the wires, and the x axis nearly perpendicular to the centermost strip. Thus, the wires measure the local y coordinate, and the strips dominate the measurement of the local x coordinate.

The readout of a CSC is triggered by the presence of anode and cathode local charged track patterns, referred to as ALCT and CLCT, respectively, which are defined in the trigger logic [5, 6]. A set of regional processors called the CSC Track Finder [7] builds the CSC muon trigger from the trigger primitives generated by individual chambers and sends it to the global muon trigger processor. For CRAFT, events were recorded with a very loose CSC trigger based on the logical “OR” of the trigger signals of all individual chambers. The rate of this loose trigger was about 60 Hz.

The ALCT wire patterns and the CLCT strip patterns were designed to be efficient only for muons originating from the interaction point. The range of track inclination (dy/dz in local coordinates) which should give efficient ALCT response is $-0.69 < dy/dz < 0$ for smaller chambers, and $-1.97 < dy/dz < 0$ for larger chambers. (The minus sign is a matter of convention.) Similarly, for the CLCT response the range is $|dx/dz| < 0.24$ for smaller, and 0.63 for larger chambers. For collision data, the muons will naturally have inclination angles within these ranges. Muons from cosmic rays, however, arrive with a much wider angular distribution.

The wire group signal is relatively fast and serves to establish the beam crossing number (BX) for a signal. Usually the anode signal extends over only one or two 25 ns beam crossings. The cathode strip signal is integrated and extends over several hundred nanoseconds. The shape of the cathode pulse can be used to infer the time of the signal to a fraction of a beam crossing number. To this end, the pulse is sampled every 50 ns (2 BX) with the results from eight time slices stored in a switched capacitor array (SCA). The arrival of the pulse is arranged so that the first two time bins are free from signal, allowing a dynamical estimate of the signal base line. A good description of the pulse shape recorded in the SCA is given by a 5-pole semi-Gaussian function:

$$S(t) \propto \left(\frac{t - T_S}{T_0} \right)^4 \exp \left[-\frac{(t - T_S)}{T_0} \right]$$

valid for $t > T_S$, the start time. Given the fixed exponent of the first factor, the shape of the pulse is determined by the decay constant T_0 , and the maximum occurs at $t = T_S + 4T_0$. Cross-talk is approximately 12% of the signal and is taken into account when calculating strip coordinates [4].

The assembly of the CSCs included a comprehensive commissioning regimen to verify chamber performance during production. This set of tests was performed again on each chamber upon arrival at CERN, and multiple times following installation on the endcap disks on the surface during 2005-7. In 2007, the disks were lowered into the CMS cavern at Point 5, and the full set of services and infrastructure became available early in 2008. At this time, the scope of the commissioning program was expanded from checking one chamber at a time to covering the entire set of 468 chambers as a subdetector system.

The commissioning effort included the following tasks: establishing inter-component communication, loading new versions of firmware on the electronics boards, turning on and configuring all components in a robust way, and measuring the parameters necessary to ensure synchronization of the system. The development of a suite of software tools was essential to bring the CSC system online. During CRAFT, the CSCs were included in the global readout about 80% of the time, and more than 96% of the readout channels were live. Figure 2 shows that hits could be reconstructed successfully in nearly all of the chambers. The chambers that did not provide data during CRAFT have been repaired since then.

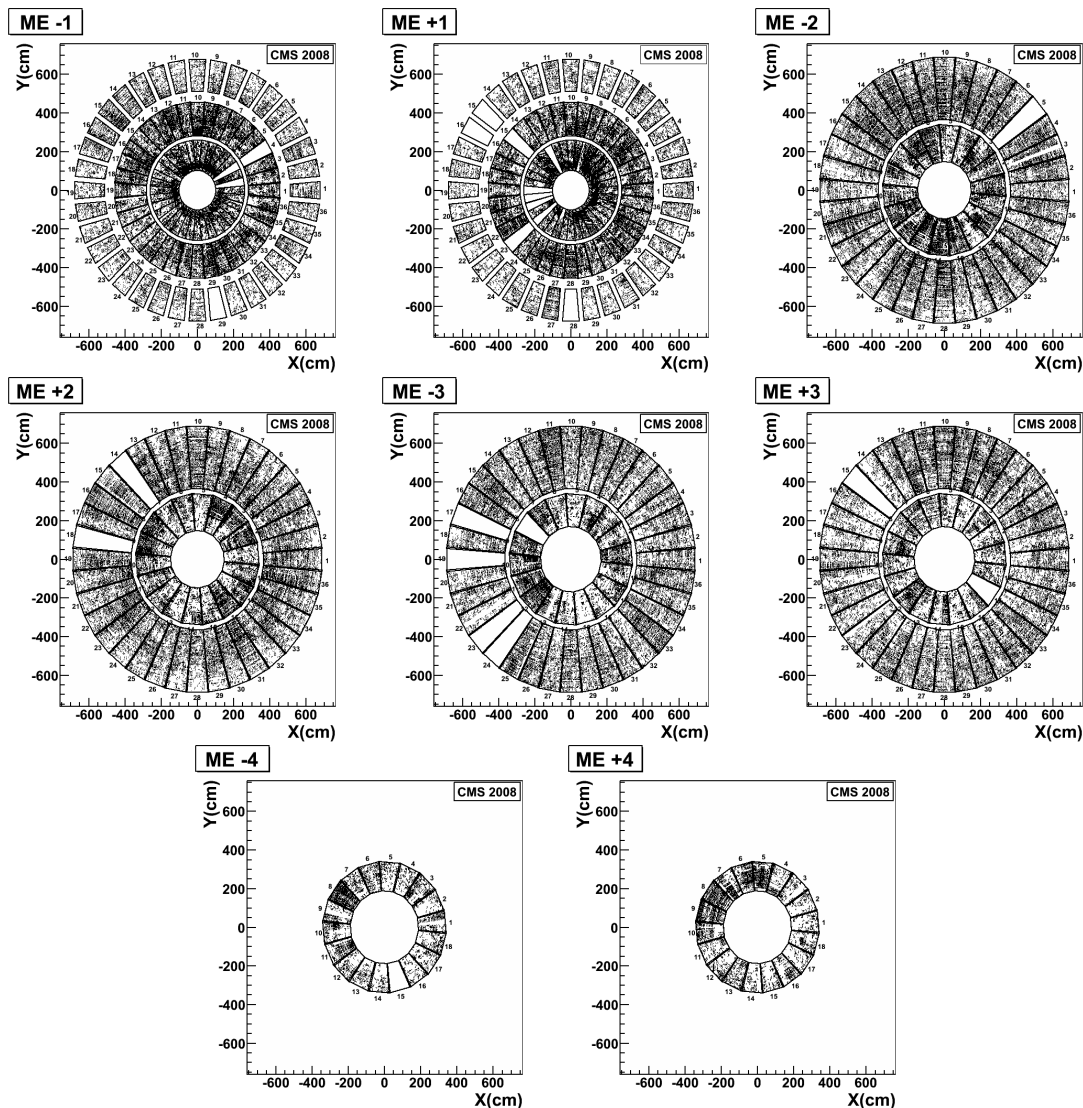


Figure 2. Distributions of hits reconstructed from a portion of the CRAFT data. Nearly all of the chambers were fully operational. A few inoperative chambers can be seen as white trapezoids; very thin white trapezoids indicate missing signals from a group of 16 strips.

3 Reconstruction of muon track segments

Raw data from the detector are unpacked offline into integer-based objects called “digis.” There are digi collections for the strip signals, the wire signals, and the local charged tracks (LCTs). The information stored in the digis is processed to produce a collection of objects called “rechits” with measured x and y coordinates at a known z coordinate. These represent the measurement of the intersection point between the track and a CSC layer. The rechits reconstructed in a given chamber are used to form a straight-line segment, which is fit to provide a measure of the muon trajectory in the chamber. Only one rechit is used from any given layer, and at least three rechits are required. The majority of segments have six rechits, while a modest fraction have fewer due to the impact of

δ -ray electrons and the boundaries of the chamber. These segments are used to seed the reconstruction of muon tracks based on muon chamber data only — these are called “stand-alone muons” [8]. Due to the very broad range of cosmic ray incident angles, only a small fraction of the stand-alone muons can be matched to reconstructed tracks in the silicon tracker, especially in the endcaps.

Simulated data sets were produced using a Monte Carlo event generator [9] which is configured to reproduce the CRAFT data as closely as possible. The CSC detector simulation reproduced approximately the number and distribution of inoperative chambers. The simulated data, the reconstructed CRAFT data, and the results presented in this paper are based on CMS reconstruction code releases dating from the spring of 2009.

4 Basic information from cosmic rays

Most cosmic ray muons above ground have an energy of at most a few GeV [10]. In the underground cavern at Point 5, the energy spectrum is shifted to somewhat higher values. Muons must have energies of at least a few GeV in order to pass through three consecutive CSC stations, since the steel disks between them are approximately $34 X_0$ thick. Most reconstructed muons have only a few GeV, so multiple scattering in the steel yoke can displace the muon’s trajectory by several centimeters with respect to the ideal trajectory.

Most of the muons triggered in the endcaps are not useful because their trajectories are steeply inclined or pass through only an edge of one of the endcaps. Only a minute fraction of the recorded cosmic ray muons follow a useful path through the endcaps, and satisfy the nominal geometric requirements for the efficient triggering and readout of the CSCs, as explained in detail below.

In order to secure a sample of useful events, a filter was applied to the primary data set to select events in which at least three chambers had hits, and in which at least two segments had been reconstructed. Events with very many rechits or segments were excluded, since they were likely to contain muon-induced showers. These criteria reduced the data sample with CSC triggers by a factor of twenty, and enabled direct comparisons of the simulated data to the CRAFT data.

Distributions of the total number of rechits per event and the number of segments per event are shown in figure 3. The requirement of three chambers with hits suppresses entries at the low end of these distributions. In the left-hand plot, the spikes at 18 and 24 rechits correspond to muons which have passed through three and four chambers.

Further information about the reconstructed segments is shown in figure 4. The first plot shows the number of hits on a segment, which must be at least three and cannot be more than six. Most segments have one rechit in every layer, and this is well reproduced by the simulation. The second and third plots show the inclinations of the segments, namely, the polar angle (“global theta”) and the azimuthal angle (“global phi”). These distributions reflect the vertical nature of the cosmic ray flux as well as the geometry of the muon endcap detector, and are fairly well reproduced by the simulation.

Finally, basic distributions for stand-alone muons in the endcaps are presented in figure 5. The first plot shows the distribution of the number of CSC rechits on the track. The distribution of simulated events differs from the CRAFT distribution in part because the residual misalignments were not fully expressed in the simulation. The second plot shows the distribution of polar angles

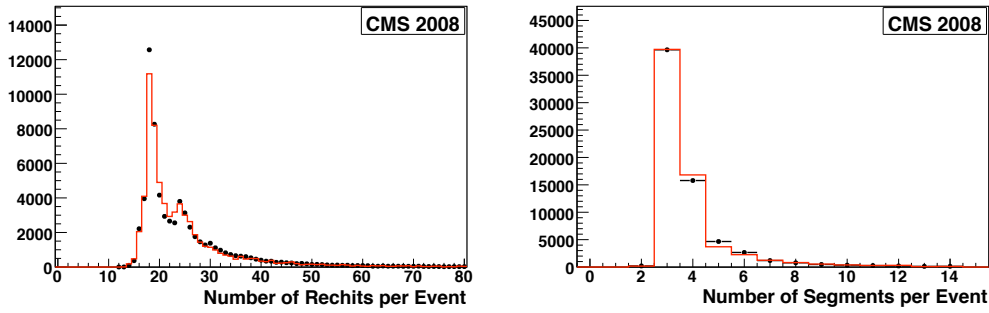


Figure 3. A comparison of the simulated events (solid line histogram) to the CRAFT events (points) for simple global quantities. Left: total number of rechits per event. Right: total number of segments per event.

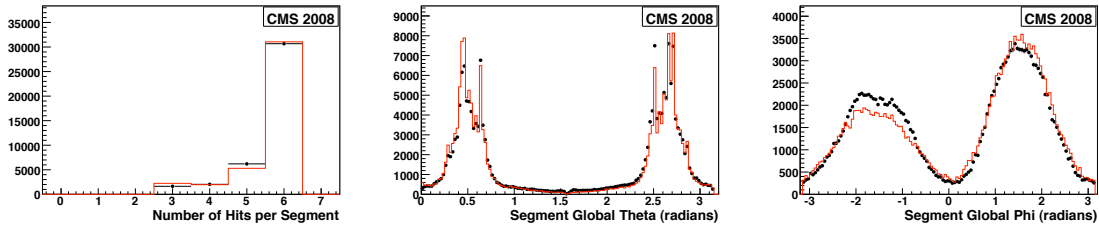


Figure 4. A comparison of the simulated events to the CRAFT events for reconstructed segment quantities. Left: number of hits per segment. Middle: global polar angle. The two endcaps are clearly visible (ME+ at $\theta \approx 0.5$ and ME- at $\theta \approx 2.7$). The narrow spikes are defined by the boundaries of the CSC rings and the event selection requirements. Right: global azimuthal angle. The bump at $\phi \approx 1.8$ corresponds to the upward vertical direction, and $\phi \approx -1.8$, to the downward.

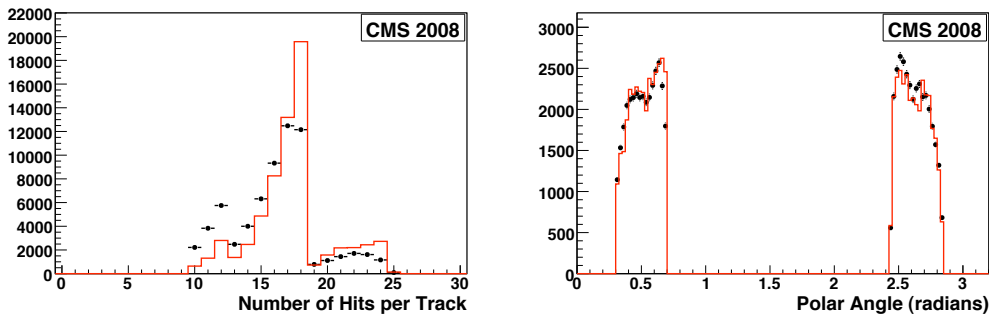


Figure 5. A comparison of the simulated events to the CRAFT events for stand-alone muon tracks. Left: number of hits per track. Right: global polar angle.

computed at the point on the stand-alone muon track closest to the center of the detector. The agreement is very good.

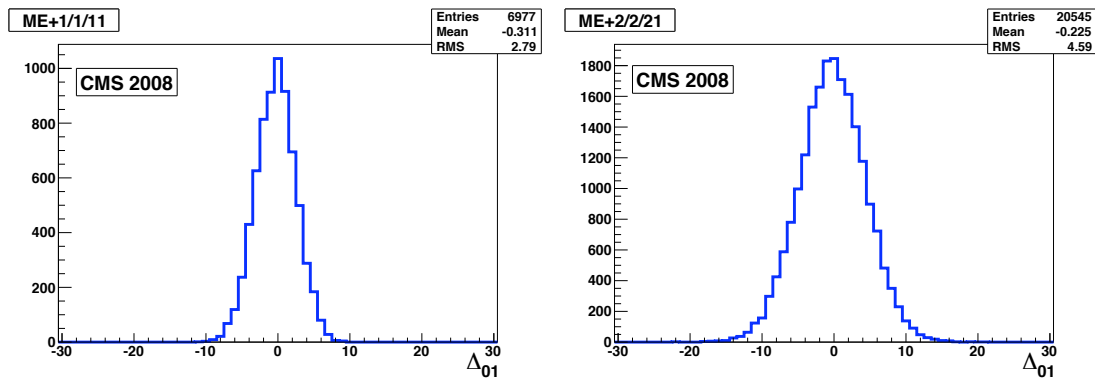


Figure 6. Two examples of Δ_{01} distributions, where Δ_{01} is the difference in the first two ADC readings for a strip. On the left, a small chamber (ME+1/1/11), and on the right, a large chamber (ME+2/2/21).

5 Noise

An assessment of the fraction of non-functional and noisy channels must be made before any discussion of efficiencies or resolution. Setting aside the few chambers that were turned off due to problems with high voltage, low voltage, or a very small number of malfunctioning electronics boards, the number of anode wire and cathode strip channels that failed to give data were below 1% of the total. Given the six-layer redundancy of each chamber, and the redundancy of the four disks in each endcap, the impact of these very few dead channels is negligible.

Noise can have two different deleterious effects, in principle: it can generate extra hits which interfere with the reconstruction of muon tracks, and it can smear or distort the measurement of the charge registered on the strips, thereby smearing or distorting the coordinates calculated from the strip information. We have used the CRAFT data to make a basic assessment of the noise on both the anode wire and cathode strip channels.

The first two out of eight 50 ns time slices of a strip signal are free of signal, by design, so that an average of these two ADC values can be used as an estimate of the base line. Consequently, the difference in the ADC values recorded for the first two time bins, $Q_1 - Q_0$, should be zero, aside from any random fluctuations due to electronics noise. In order to ensure that no signal contributes to Q_1 and Q_0 , strip channels were omitted which have a sum of charges 13 ADC counts or more above base line.

The rms of the distribution of $\Delta_{01} \equiv Q_1 - Q_0$, σ_{01} , is taken to be a measure of noise, and was obtained for all sets of 16 strip channels handled by the cathode front-end boards, for all chambers. Figure 6 displays two example distributions for Δ_{01} showing that the distributions have no tails or asymmetry. One ADC count corresponds to approximately 0.54 fC.

Figure 7 shows the distribution of all σ_{01} values which are typically about 3 ADC counts or slightly larger; the spread of the distribution is small indicating excellent uniformity. There are no large values, indicating no oscillating or otherwise noisy channels. The two populations in figure 7 correspond to the smaller and larger chambers.

The time integration of the amplifier leads to an auto-correlation manifested as a correlation coefficient of 0.26 between consecutive time slices which reduces slightly σ_{01} with respect to the uncorrelated case. We repeated this noise analysis using the first and the last time bins, and found

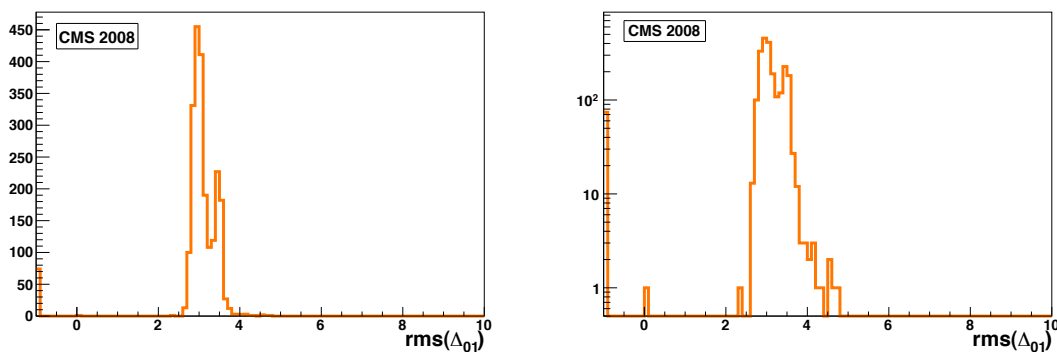


Figure 7. Distribution of all σ_{01} values, i.e., the rms of the difference in the first two ADC readings, on a linear scale (left) and a log scale (right). There is one entry per chamber, and the entries at $\Delta_{01} = -1$ correspond to channels that were turned off. The single entry at $\Delta_{01} = 0$ comes from a single nonfunctional channel.

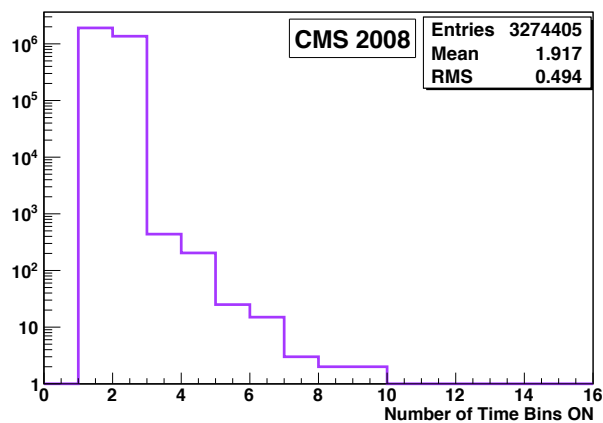


Figure 8. A semi-log plot of N_{on} (the number of time bins for which there is signal) for all anode wire channels in ME-2/1/9.

that the rms values increased by about 10%, due partly to the lack of correlation between the first and last time slices. We also observed some sensitivity to signal in the last time slice, due to cross-talk, which explains the rest of the 10% increase with respect to σ_{01} .

The anode wire signals normally extend over one or two 25 ns time bins. A noisy channel, however, will rise above threshold in more time bins, so a useful quantity to identify noisy channels is the number of time bins for which a given anode hit is *on*, denoted here by N_{on} . The distribution of N_{on} for all anode channels in a particular chamber is shown in figure 8, on a semi-log plot. A very small tail for $N_{\text{on}} > 2$ can be seen. The number of noisy anode wire channels is estimated to be less than 0.1%.

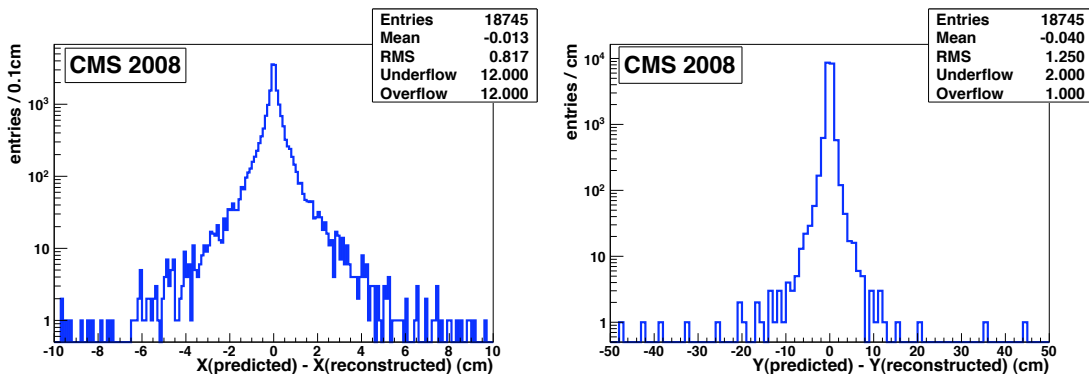


Figure 9. Differences between the predicted positions of a segment and the position of the reconstructed segment in the probe chamber. Δx is on the left, and Δy is on the right, where x and y are local coordinates. x is measured primarily by the strips, and y by the wires.

6 Efficiency

The goal of this study is to measure the absolute efficiency of each step in the reconstruction of muons in the CSCs, from the generation of ALCTs and CLCTs to segment reconstruction. By design, for good muons coming from the interaction point, all steps should be highly efficient. The method described here uses two chambers to “tag” a muon that passes through a designated “probe” chamber. When computing the efficiency of each step, the same tagged sample (i.e., the denominator in the efficiency calculation) is used for all steps.

For efficiency measurements, we need a well-defined muon track which is independent of the measurements in the chamber under investigation. We use muon tracks reconstructed in several CSCs without any information from the silicon tracker. The number of useful stand-alone muons is adequate for the present purposes, thanks to the redundancy of the muon endcap system. To minimize the impact of multiple scattering, energy loss, and tracking in a strong magnetic field, a chamber is probed only if it lies between the endpoints of the track. Consequently, at least two independent measurements of the muon track are needed, and only interpolation and not extrapolation to the probe chamber is used. Some rings, namely $ME\pm 1/1$, $ME\pm 4/1$ and $ME-3/2$ cannot be covered by this study, although hits in the CMS Resistive Plate Chambers allow coverage of $ME+3/2$.

A typical event selected for these efficiency measurements contains three or four CSCs contributing to a good stand-alone muon track. Since the trigger efficiency is generally high (see below), and a trigger from any one of these chambers sufficed to produce a trigger for read out of CMS, we assume that any trigger bias in these results is negligible.

We place cuts on the predicted position of the muon in the probe chamber to avoid losses due to insensitive regions at the periphery of the chamber and at the boundaries of the high voltage segments. Figure 9 shows distributions of the difference between the measured position of a segment in the probe chamber and the predicted position, obtained by propagating the muon track from another station to the probe chamber, taking the magnetic field, multiple scattering and energy loss into account. In this figure, the local coordinate x runs parallel to the wires, and is measured primarily by the strips, while y runs perpendicular to the wires, and is measured by the wire signals. According to these distributions, nearly all of the tracks fall within 10 cm of the predicted position.

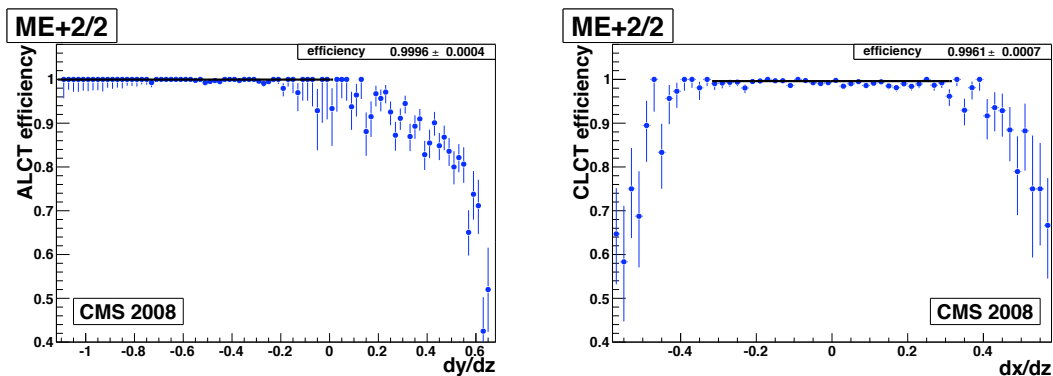


Figure 10. Left: ALCT efficiency as a function of the track inclination, dy/dz in local coordinates. Right: CLCT efficiency as a function of the track inclination, dx/dz in local coordinates.

A set of stringent criteria is used to select “good” tracks for the denominator of all efficiency calculations. Only one stand-alone muon track is allowed in an endcap. This track has to have a minimum number of hits, and to be reconstructed well, as indicated by the χ^2 and the relative error on the momentum. The momentum is required to be in the range $25 < p < 100 \text{ GeV}/c$. A track satisfying these requirements is propagated to a designated ring of CSC chambers to ascertain which chamber is the probe chamber. If the interpolated point lies within 10 cm of the edges of the chamber or dead regions defined by high voltage segment boundaries, then the chamber is skipped. The tracks which pass all of these criteria are the “probe” tracks.

The following sections report the details of the measurements and the values of the efficiency for each step in the CSC local reconstruction.

6.1 LCT efficiencies

The ALCT and CLCT efficiencies are measured independently. For a given chamber, the ALCT and CLCT digis are unpacked to test for the presence of a valid ALCT or CLCT. If they are present anywhere in the chamber, then the trial is a “success” and the chamber is “efficient” for that event.

To suppress the muons which are not likely to fire the ALCT and/or CLCT triggers, we apply cuts on the slopes of the muon tracks interpolated through the chamber:

$$-0.8 < \frac{dy}{dz} < -0.1 \quad \text{and} \quad \left| \frac{dx}{dz} \right| < 0.2.$$

One could adjust these ranges for the various rings of chambers, but the impact on the efficiency measurements is negligible. All the efficiencies measured with CRAFT data include these requirements in the event selection.

The variation of the ALCT efficiency as a function of dy/dz is shown in figure 10 (left). For this figure, the cut on dy/dz was not applied, although the cut on dx/dz was applied. Similarly, the variation of the CLCT efficiency as a function of dx/dz is shown in figure 10 (right), with the cut on dx/dz relaxed, and the cut on dy/dz applied. The results shown in these plots are based on data from chambers 5–13 in ring ME+2/2 which are known to have been operating well during CRAFT. In both figures, clear plateaus can be seen which were fit with level functions to ascertain

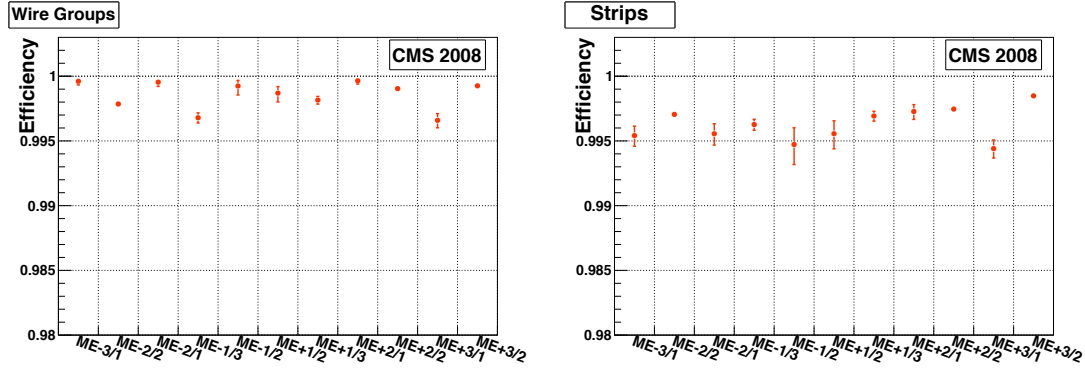


Figure 11. A summary of wire group (left) and strip (right) digi efficiencies, over all functioning chambers in a ring. Some rings are inaccessible in this study with CRAFT data.

the efficiency. Very high values in excess of 0.99 are observed, confirming earlier results obtained with cosmic rays [11].

6.2 Strip and wire group efficiencies

The presence of an ALCT and CLCT should trigger the readout of the chamber, and hence, signals on the wires and strips should be present in the raw data, or equivalently, in the strip and wire digis. The efficiency for strip and wire digis are measured independently. The probe is given by a good track passing through the given chamber.

The efficiencies of strips, wire groups and rechits are defined naturally per layer. If the layer measurements are independent, then the average efficiency per chamber would be

$$\bar{\epsilon} = \frac{\sum_i \epsilon_i}{L} = \frac{\sum_i n_i}{N \times L} \tag{6.1}$$

with an estimated uncertainty of

$$\Delta\bar{\epsilon} = \sqrt{\frac{\bar{\epsilon} \times (1 - \bar{\epsilon})}{L \times N}}, \tag{6.2}$$

where $L = 6$ is the number of layers, ϵ_i is the efficiency in layer i ($i = 1, \dots, 6$), n_i is the number of efficient cases (“successes”) for layer i , and N is the number of probe tracks. In principle, there might be events with a simultaneous loss of information from all six layers, in which case eq. (6.2) is incorrect. There is no evidence for any such correlated losses.

The average wire group and strip digi efficiencies are shown in figure 11. Typically, all six layers have high efficiency, greater than 99.4%.

6.3 Rechit efficiency

The efficiency for reconstructing a rechit is measured for each layer in a chamber. The chamber is efficient if the rechits are found in a given layer - there is no requirement on the distance between the rechit and the interpolated point. Also, no quality requirements are placed on the individual rechits as part of the measurement of rechit efficiency.

The rechit efficiency will be a convolution of the strip and wire group digi efficiencies. It might also depend on some of the details of the rechit reconstruction algorithm, especially as regards

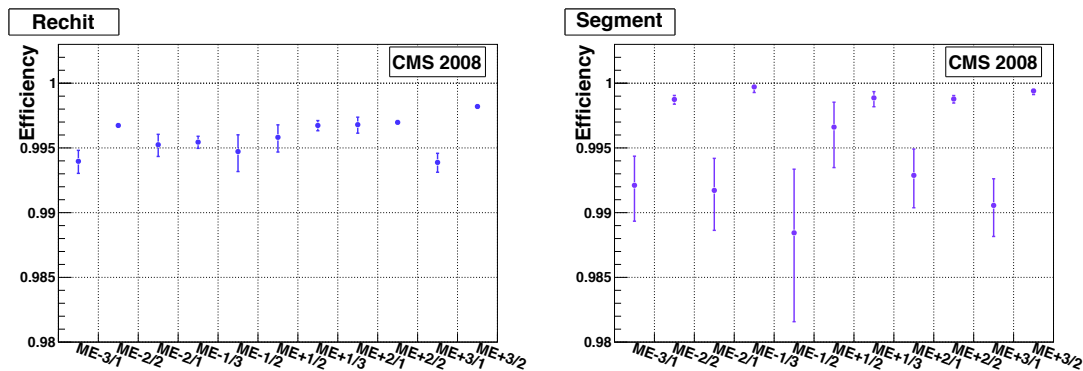


Figure 12. Summaries of rechit and segment efficiencies, analogous to figure 11.

quality or other criteria applied to the strip and wire signals. The rechit efficiency for all the accessible CSC rings is above 99.3%, as shown in figure 12 (left).

6.4 Segment efficiency

It should be possible to build a segment if at least three good rechits are recorded along the muon trajectory. The chamber is efficient if a segment has been reconstructed. No matching criteria have been applied because the reconstructed segments are found close to the extrapolated positions, as shown in figure 9.

Ideally, the segment efficiency would be related in a simple and direct way to the rechit efficiency. The segment reconstruction algorithm, however, also places requirements on the rechits used to build segments. It does not find segments in chambers with very many hits, due to prohibitive combinatorial problems — this will register as an inefficiency in the present study. The segment efficiency for all the rings in the CSC system is shown in figure 12 (right). For cosmic rays, the segment efficiency is above 98.5%.

6.5 Attachment efficiency

The attachment efficiency is a characteristic of the segment builder. It is defined as the probability of the segment to use a rechit from a given layer if there are rechits in that layer. The segment finder could reject some rechits if their quality were poor, or if they were producing a bad fit, so one can anticipate a small inefficiency with respect to the efficiency for producing rechits. What is important is that this inefficiency should be the same for all layers. Any significant variation with layer number would be a hint of a problem — for example, an unacceptable dependence on the track angle. Figure 13 shows that there is no bias in the CRAFT data.

In summary, all the basic efficiencies have been shown to be high, for chambers in good operating condition during CRAFT, as listed in table 2.

7 Resolution

The CRAFT data were used to study and measure the spatial resolution of the CSCs as they are meant to be operated for early physics. (The current high voltage settings are intentionally lower

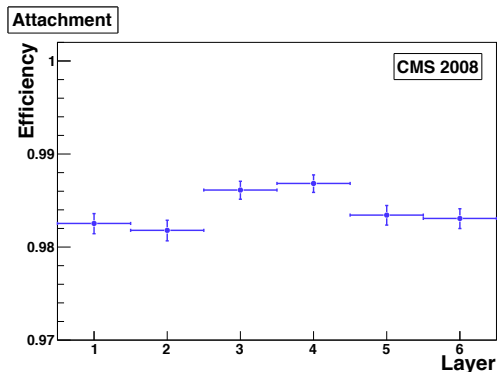


Figure 13. The attachment efficiency for each layer.

Table 2. Summary of efficiencies for chambers in good operating condition.

quantity	typical efficiency (%)
ALCT	> 99.9
CLCT	> 99.5
wire digis	> 99.5
strip digi	> 99.4
rechit	> 99.3
segment	> 98.5

than what was used for the test beam studies, in order to avoid aging the chambers unnecessarily during commissioning periods. This has a significant impact on the spatial resolution, as described below.) The purpose of this study is to verify that all working chambers perform as they should, before colliding beams commence. Earlier studies of CSC spatial resolution can be found in ref. [12].

7.1 Methodology

The *resolution* is the typical measurement error. It is determined by the design parameters of the chamber (width of the cathode strip, distance to the anode wire plane, high voltage, anode wire radius and pitch, gas mixture, electronics noise and cross talk) as well as certain characteristics of each muon track (angle, position with respect to the center of the struck strip, and amount of charge collected), the physics of multi-wire proportional chambers (electron diffusion, magnetic field influence) and the reconstruction (reduction of data and knowledge of misalignments). The distribution of hit residuals with respect to the muon trajectory can give a good measure of the resolution. A *residual* is the difference between the measured coordinate and the predicted coordinate.

For the purposes of the study, the coordinate of interest is the coordinate measured by the strips. In global coordinates, this would be $R\phi$, but most of the results presented here are expressed in *strip coordinates*. The strip coordinate, s , is the $R\phi$ coordinate relative to the center of the strip, divided by the strip width at the position of the hit. Apart from resolution effects, one has $-0.5 \leq s \leq 0.5$. In order to obtain a resolution in physical units, we multiply by the mean width of

a strip in the given chamber, reported in table 1.

The residuals distribution is not Gaussian, in general, so one must settle on a measure of the residuals distribution to be identified with the “resolution” of the given chamber. We fit the distribution with a sum of two Gaussian functions, with zero mean, using the functional form:

$$f(x) \equiv \frac{A_1}{\sqrt{2\pi}\sigma_1} \exp\left(\frac{-x^2}{2\sigma_1^2}\right) + \frac{A_2}{\sqrt{2\pi}\sigma_2} \exp\left(\frac{-x^2}{2\sigma_2^2}\right) \quad (7.1)$$

where values for the parameters σ_1 , σ_2 , A_1 and A_2 are obtained from the fit. We take the resolution to be:

$$\bar{\sigma} = \sqrt{\frac{A_1\sigma_1^2 + A_2\sigma_2^2}{A_1 + A_2}}. \quad (7.2)$$

If one Gaussian suffices, then we take simply the σ parameter of the single Gaussian. We do not take the rms as the residual distributions often have long non-Gaussian tails which inflate the rms - these tails are caused by δ -ray electrons and fall outside a discussion of the core resolution. The residuals distributions of eight chamber types with fits to eq. (7.1) are given in figure 14.

As defined, the resolution $\bar{\sigma}$ pertains to a hit in a *single layer*. The resolution of a chamber is more complicated, since it depends on the number of hits in the segment, the direction of the segment, the generally non-normal angle between wire groups and strips, and the fact that the strips are staggered layer-by-layer for all chambers except ME \pm 1/1. We can take the special case of segments with six hits that are normal to the chamber and pass through the center. If the residuals distribution for hits near the edge of a strip ($|s| > 0.25$) has Gaussian width σ_e , and for hits near the center of a strip ($|s| < 0.25$), σ_c , then to a good approximation, the resolution for the segment is

$$\sigma_{\text{seg}} = \left(\frac{3}{\sigma_e^2} + \frac{3}{\sigma_c^2}\right)^{-1/2}. \quad (7.3)$$

We will use this expression to characterize the chamber resolution.

Another method for measuring the resolution does not rely on the residuals of a single layer, but rather on the value of χ^2 for the linear fit to all six hits. We define the *unweighted* χ^2 as follows:

$$\chi_0^2 \equiv \sum_{i=1}^6 [s_i - (a + bi)]^2 \quad (7.4)$$

where a and b are free parameters, and the layer number i plays the role of the z coordinate. Since there are two free parameters and six data points, $\langle \chi_0^2 \rangle = 4\sigma_0^2$, where σ_0 is the effective uncertainty on s_i .

We do not have a good exterior measure of the position of the muon, so we have to use the segment itself. We fit the hits in layers 1, 2, 4, 5 and 6 to a straight line to predict the “correct” position in layer 3, and then compare to the measured position in layer 3. The estimated error for those five hits are used in the fit. Monte Carlo studies show that the width of the residuals distribution is inflated by about 10% due to the measurement error from the five-hit fit; this uncertainty is larger for layers 1, 2, 5 or 6. We do not remove this 10% inflation for the results reported in this paper. Also, no attempt was made to remove layer-by-layer misalignments, as these are known to be small compared to the resolution.

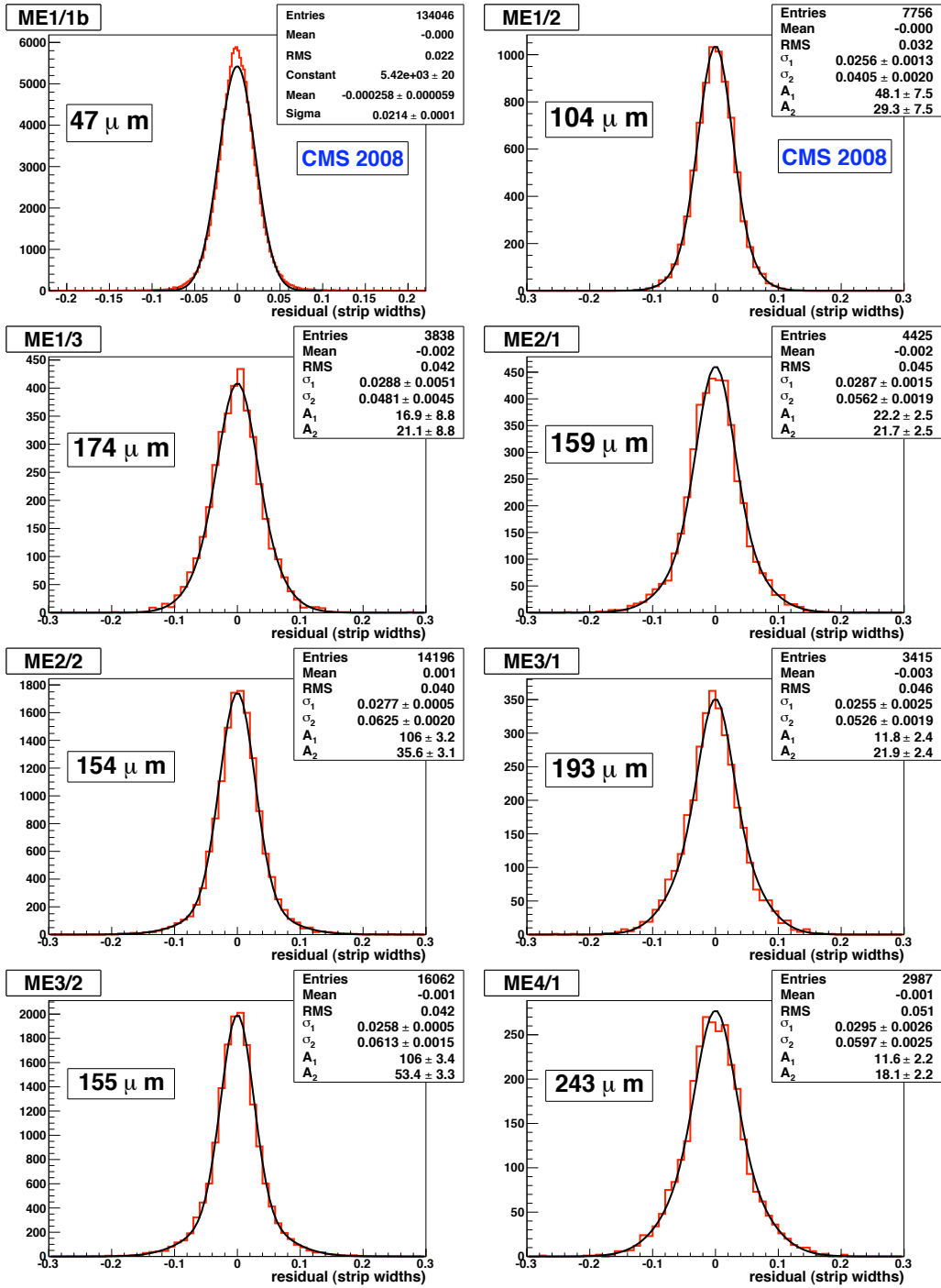


Figure 14. Distributions of residuals fit to the double-Gaussian function given in eq. (7.1), except for the ME \pm 1/1 chambers, which are fit to a single Gaussian. The numbers in boxes correspond to the *chamber resolution*, obtained from eq. (7.3) and the average strip widths given in table 1.

7.2 Results from CRAFT

The resolution is known to vary with several quantities, including the charge recorded for that hit, the position within the strip, the physical width of the strip, the inclination of the track and the magnetic field, among others [13–15]. The charge usually extends across three strips, which we label Q_L , Q_C and Q_R , where by definition the charge on the central strip is larger than that on the left and right side strips. We take the charge on these three strips, measured for three consecutive time slices centered on the peak of the signal, and form the sum, $Q_{3\times 3}$ [12].

Events were selected which contained a good segment from which residuals distributions for layer 3 could be formed. A good segment was one which contained six rechits and $\chi^2 < 200$ (unreduced). An event was selected if it contained at least one good segment. In order to retain only clean events, any event with more than eight segments of any quality were rejected, as well as events with more than fifty rechits. The event was also rejected if any chamber contained more than four segments of any quality.

Further criteria were applied when filling residuals distributions:

1. The estimated errors on the six rechits have to be smaller than 0.2 strip widths. This eliminates rechits based on a single strip or anomalous charge distributions.
2. The sum of charges for three strips and three time slices for layer 3 could not be too small or too large: $250 < Q_{3\times 3} < 1000$ ADC counts (4000 ADC counts for the $ME\pm 1/1$ chambers).
3. The segment inclination should correspond to tracks originating roughly from the interaction point:

$$-1 < \frac{dy}{dz} < -0.15 \quad \text{and} \quad \left| \frac{dx}{dz} \right| < 0.15. \quad (7.5)$$

4. The strip coordinates were fit to a straight line. The resulting χ^2 values were required to be less than 9 for the 5-hit fit, and less than 50 for the 6-hit fit.

These cuts were relaxed singly when checking the impact of these criteria.

The registered charge depends on several factors, including the gas composition, pressure, high voltage, amplifier gain, and the ionization of the gas by the muon. A distribution of $Q_{3\times 3}$ for the CRAFT data is shown in figure 15 (left). The distribution has a long tail, similar to that expected from the Landau distribution.

The variation of the resolution as a function of charge is illustrated in figure 15 (right). Chambers in rings $ME\pm 2/2$ and $ME\pm 3/2$ were selected for this plot, since they have the largest number of events in CRAFT. The cuts on the χ^2 of the fits to strip coordinates were relaxed for this study, so that the impact of δ -ray electrons is evident at large ionization charge. If the cuts are imposed, then the rise for $Q_{3\times 3} > 800$ ADC counts is eliminated.

Another demonstration of the sensitivity of the resolution to charge is provided by two runs taken outside of the CRAFT exercise, in which the high voltage was raised by 50 V from 3600 V. Since the number of events was modest, the event and segment selection was somewhat looser than described above. The increase in the observed charge is about 20% and the improvement in resolution is about 20%, consistent with expectations - see figure 16.

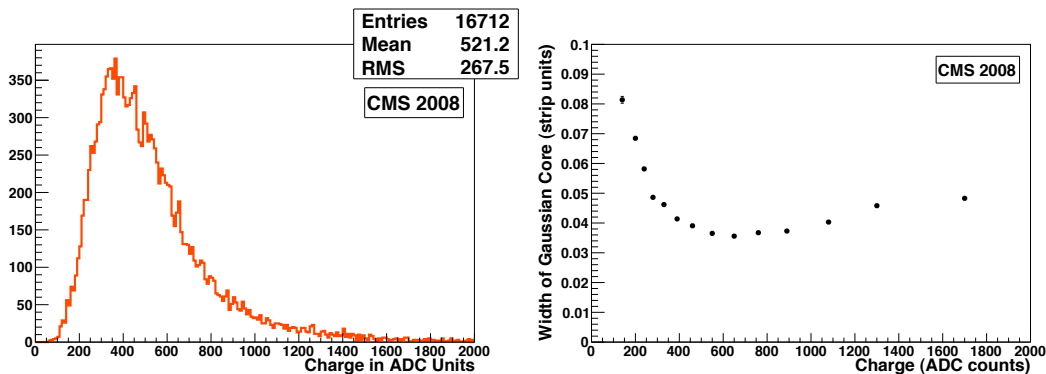


Figure 15. Left: Observed charge distribution, $Q_{3 \times 3}$, in ADC counts. Right: Variation of the *per layer* resolution as a function of $Q_{3 \times 3}$. This measurement was made using chambers in $ME \pm 2/2$ and $ME \pm 3/2$; other chambers give very similar results.

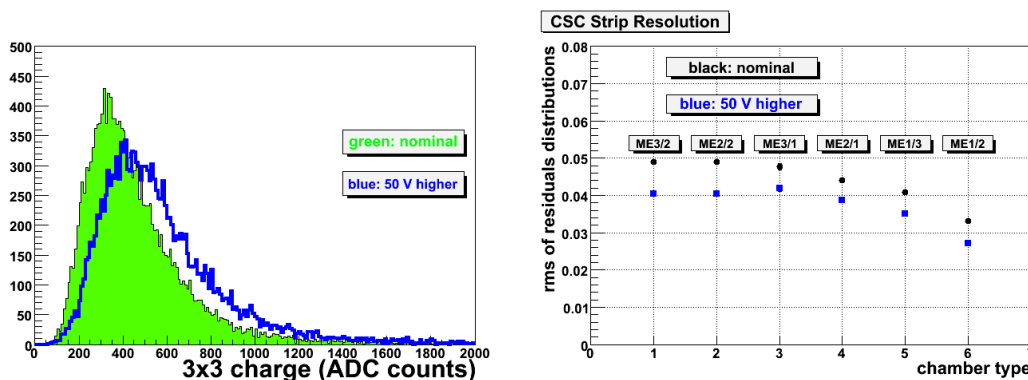


Figure 16. Left: Charge distributions for two consecutive runs. The solid histogram corresponds to the nominal setting, and the open histogram corresponds to an increase of 50 V. Right: Comparison of the *per layer* resolution for the same two runs, in strip units.

The variation of the resolution with the position within a strip, s , is shown in figure 17 (left). For the $ME \pm 2/2$ chambers, the resolution in the center of the strip is worse by about a factor of two than at the edge. This variation is weaker for chambers with thinner strips, such as $ME \pm 1/2$ and $ME \pm 1/1$.

Most of the analysis presented here is done in terms of the normalized strip width, s . The physical width of the strip matters, too. For broad strips, most of the charge is collected on the central strip, leaving a small amount for Q_L and Q_R , leading to a poorer resolution. For this reason, the smaller chambers in $ME \pm 1/1$ have a much better resolution than the larger chambers. Within a chamber, there is a mild variation of the resolution along the strip, since the strip is narrower at the narrow end of the chamber and wider at the broad end.

The results described above were derived for muon trajectories that were nearly perpendicular to the strips. For low-momentum muons coming from the interaction point, however, more oblique trajectories are possible. We have observed a clear variation of the resolution as a function of dx/dz in chambers from ring $ME \pm 2/2$, see figure 17 (right). For all other results reported in this note, a tight cut on $|dx/dz|$ has been applied, as listed in eq. (7.5).

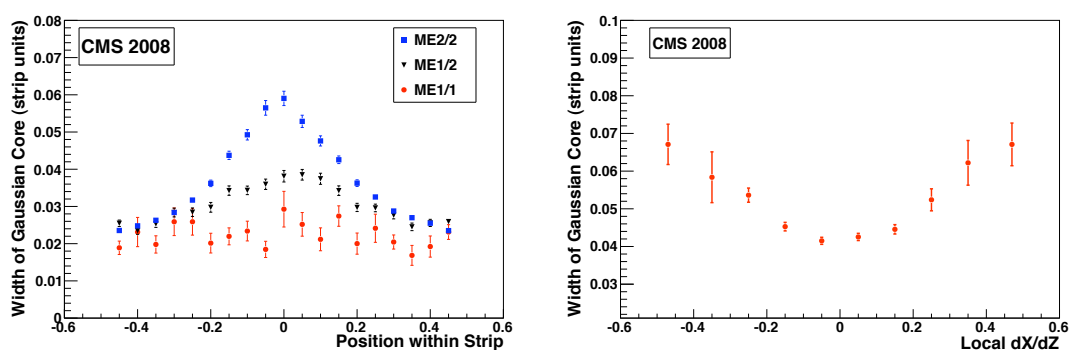


Figure 17. Left: Variation of the *per layer* resolution as a function of s , the position within the strip, for three different types of chambers. Right: Variation as a function of local dx/dz . These measurements were done with the $ME\pm 2/2$ chambers.

7.3 Measurements of the resolution

The results in the previous section demonstrate the expected behavior of the resolution. In this section, we quantify the resolution of the CSCs, as measured with CRAFT data, in order to verify that they are performing as designed.

Residuals distributions for chambers in each ring were fit to the sum of two Gaussian functions as in eq. (7.1), and the resolution computed according to eq. (7.2). These distributions are shown in figure 14, and table 3 lists the *per layer* resolution obtained in this manner. The values given in μm are obtained by multiplying the resolution in strip widths by the average width of the strip (see table 1).

The estimated uncertainty is computed taking into account variations as a function of charge, position within a strip, and strip width. Distributions of normalized residuals (“pull distributions”) allow us to check those calculations. A summary of the pulls for all chamber types is given in table 3. Overall, the pulls are somewhat too wide, especially for the $ME\pm 1/1$ chambers, indicating that the uncertainties are slightly underestimated. It will be possible to adjust the error estimates on the basis of the CRAFT data.

We formed distributions of χ_0^2 defined in eq. (7.4) for each chamber type, computing σ_0 and converting to an uncertainty in μm using the average physical strip width. The results are listed in table 3. These values agree well with the values obtained from the fit to Gaussian functions.

The resolution of a chamber, given six good rechits, can be estimated on the basis of the *per layer* resolution. One can simply take the numbers listed in table 3 and divide by $\sqrt{6}$, or one can perform a slightly more refined analysis indicated by eq. (7.3). The latter gives systematically lower values for the resolution than the former. Table 4 lists both sets of values, which can be compared to the design values [4]. Most observed values are somewhat higher, except for the $ME\pm 1/1$ chambers, which are significantly better than design. The fact that the high voltage is set to a somewhat reduced value to reduce ageing is the primary reason for the slightly worse resolution in the non- $ME\pm 1/1$ chambers.

Table 3. Resolution *per layer* for each chamber type, and the rms of the pull distributions.

ring	resolution				pull rms
	<i>fit to two Gaussians</i>		<i>derived from χ_0^2</i>		
	strip widths	μm	strip widths	μm	
ME \pm 1/1 <i>b</i>	0.0214 \pm 0.0001	129	0.020	119	1.80 \pm 0.06
ME \pm 1/2	0.031 \pm 0.001	265	0.033	278	1.40 \pm 0.01
ME \pm 1/3	0.040 \pm 0.003	513	0.046	606	1.73 \pm 0.01
ME \pm 2/1	0.042 \pm 0.001	474	0.051	571	1.41 \pm 0.02
ME \pm 2/2	0.036 \pm 0.001	447	0.045	551	1.47 \pm 0.01
ME \pm 3/1	0.043 \pm 0.002	503	0.053	619	1.44 \pm 0.03
ME \pm 3/2	0.038 \pm 0.001	461	0.046	569	1.44 \pm 0.01
ME \pm 4/1	0.048 \pm 0.002	579	0.057	693	1.43 \pm 0.03

Table 4. Resolution *per chamber* for each chamber type.

ring	resolution (μm)		
	design	<i>per layer</i> / $\sqrt{6}$	eq. (7.3)
ME \pm 1/1 <i>b</i>	75	52	47
ME \pm 1/2	75	116	104
ME \pm 1/3	150	234	174
ME \pm 2/1	150	208	159
ME \pm 2/2	150	199	154
ME \pm 3/1	150	258	193
ME \pm 3/2	150	218	155
ME \pm 4/1	150	264	243

7.4 Special studies for ME1/1

The ME \pm 1/1 chambers play a special role. First, they provide the key measurements for the high-momentum muon tracks expected at high $|\eta|$. And second, they must operate in a very high magnetic field, which alters the drift of the electrons inside the gas layers. For these reasons, the gas gaps are smaller, the gas gain is higher, the strips are narrower, and the wires are tilted with respect to wires in the other chambers [16].

The drift of the electrons perpendicular to the anode wires depends sensitively on the magnetic field. Most of the CRAFT data were taken at full operating field, but some data were taken with zero field, and with some intermediate values. These data were analyzed to measure the resolution as a function of the magnetic field, with the results shown in figure 18 (left). For the measurements at $B \approx 2$ T and 2.9 T, the field was changing, as indicated by the horizontal error bars. The resolution is best at the maximum operating value of the field, confirming the details of the chamber design.

The radial extent of the ME \pm 1/1*b* chambers was divided into four regions in order to check

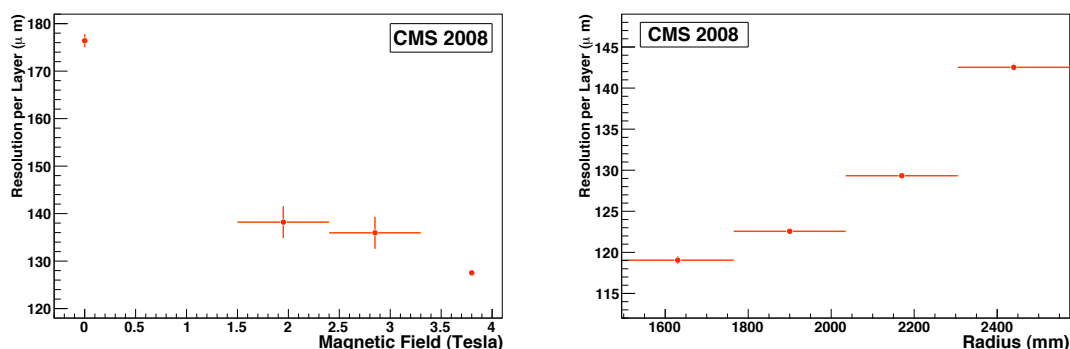


Figure 18. Left: Variation of the resolution in the $ME\pm 1/1b$ chambers as a function of magnetic field in Tesla. The horizontal error bars on the center two points reflect the changing value of the field for those data. Right: Variation of the resolution as a function of the radius (distance from the beam line).

the resolution at different radii. Figure 18 (right) shows that the resolution is best near the beam line, where it is most critical, and rises rapidly with radius. A further study of the resolution for different azimuthal regions of the $ME\pm 1/1b$ chambers shows a mild variation with the angle of the anode wires, confirming the choices made in the design of these chambers.

8 Timing

We used the CRAFT data to make some simple tests of the timing capabilities of the CSCs. The time of flight of a muon through a single chamber is quite small, essentially zero compared to the 25 ns BX spacing. Figure 19 shows the distribution of differences in measured times for layers 6 and 1, in units of 50 ns time bins. The mean is consistent with zero, and the rms is 0.214 time bins, which corresponds to 7.2 ns, or 5 ns per layer. Most segments have six rechits (cf. figure 4), so a single segment should have a time resolution of about 2 ns. This compares well with the transit time of a muon from the interaction point to the CSCs of roughly 30 ns, and of the beam crossing time of 25 ns.

Improvements in the use of the strip timing information are foreseen, based on a more detailed analysis of the subtle effects of cross talk and noise correlations, as suggested by pilot studies with test beam data. It is hoped to use this timing capability for rejecting out-of-time hits and tagging the time of the muon independently of the trigger system.

9 Summary

An assessment of the performance of the CSCs has been completed using the large CRAFT data sample recorded in fall 2008. More than 96% of the CSC muon detector system was in excellent working condition and participated in the bulk of this campaign. The simulation reproduces well distributions of basic global quantities, such as the number of hits on track segments and the angular distributions of muon tracks, observed in the data. The fraction of channels which provided no signal, or were noisy, is less than 1%. All of the essential efficiencies have been measured, ranging from the local charged tracks which trigger the chamber readout through the reconstruction of

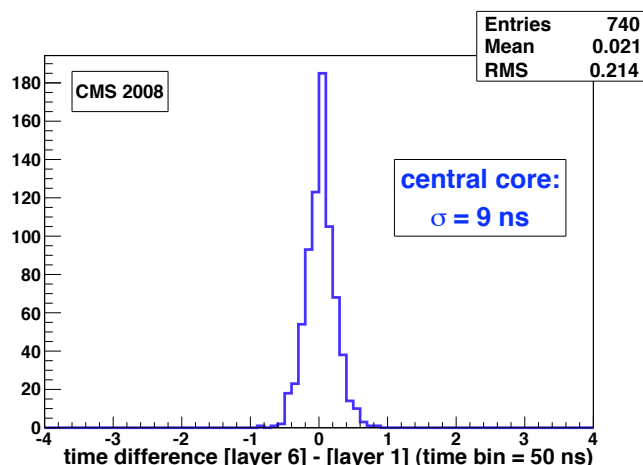


Figure 19. The difference in rechit times for layers 6 and 1 in chamber ME+3/2/9. Units are 50 ns time bins. A fit of the central core to a Gaussian function gives a width of 9 ns.

segments. These efficiencies are all very high. The position resolution has been studied, with variations observed as a function of several relevant variables, such as the charge, position within a strip, high voltage, track inclination, and in the case of the ME \pm 1/1 chambers, of the magnetic field, radius and wire tilt. The measured chamber resolutions are not quite as good as design, due to an intentional reduction of the high voltage, except for the ME \pm 1/1 chambers, which surpass the design criterion. Finally, the potential timing capabilities of the CSCs was briefly investigated.

The prospects for future studies are very good. The operating conditions of the CSC subsystem have been improved since the CRAFT data were taken, and one can anticipate that the CSC subsystem will function up to specifications once the LHC delivers collisions to CMS.

Acknowledgments

We thank the technical and administrative staff at CERN and other CMS Institutes, and acknowledge support from: FMSR (Austria); FNRS and FWO (Belgium); CNPq, CAPES, FAPERJ, and FAPESP (Brazil); MES (Bulgaria); CERN; CAS, MoST, and NSFC (China); COLCIENCIAS (Colombia); MSES (Croatia); RPF (Cyprus); Academy of Sciences and NICPB (Estonia); Academy of Finland, ME, and HIP (Finland); CEA and CNRS/IN2P3 (France); BMBF, DFG, and HGF (Germany); GSRT (Greece); OTKA and NKTH (Hungary); DAE and DST (India); IPM (Iran); SFI (Ireland); INFN (Italy); NRF (Korea); LAS (Lithuania); CINVESTAV, CONACYT, SEP, and UASLP-FAI (Mexico); PAEC (Pakistan); SCSR (Poland); FCT (Portugal); JINR (Armenia, Belarus, Georgia, Ukraine, Uzbekistan); MST and MAE (Russia); MSTDS (Serbia); MICINN and CPAN (Spain); Swiss Funding Agencies (Switzerland); NSC (Taipei); TUBITAK and TAEK (Turkey); STFC (United Kingdom); DOE and NSF (USA). Individuals have received support from the Marie-Curie IEF program (European Union); the Leventis Foundation; the A. P. Sloan Foundation; and the Alexander von Humboldt Foundation.

References

- [1] CMS collaboration, *The CMS experiment at the CERN LHC*, [2008 JINST 3 S08004](#).
- [2] L. Evans and P. Bryant eds., *LHC Machine*, [2008 JINST 3 S08001](#).
- [3] CMS collaboration, *Commissioning of the CMS experiment and the cosmic run at four tesla*, [2010 JINST 5 T03001](#).
- [4] CMS collaboration, *CMS – The Muon Project*, CERN-LHCC-97-32 (1997);
D. Acosta et al., *Large CMS cathode strip chambers: design and performance*, *Nucl. Instrum. Meth. A* **453** (2000) 182.
- [5] CMS collaboration, *CMS Physics Technical Design Report*, [CERN-LHCC-2006-001](#) (2006).
- [6] J. Hauser et al., *Experience with Trigger Electronics for the CSC System of CMS*, Proceedings of the 10th Workshop on Electronics for LHC Experiments and Future Experiments (2004).
- [7] CMS collaboration, *Performance of the CMS Level-1 trigger during commissioning with cosmic ray muons and LHC beams*, [2010 JINST 5 T03002](#).
- [8] CMS collaboration, *Performance of CMS muon reconstruction in cosmic-ray events*, [2010 JINST 5 T03022](#).
- [9] P. Biallass, T. Hebbeker and K. Hoepfner, *Simulation of Cosmic Muons and Comparison with Data from the Cosmic Challenge using Drift Tube Chambers*, [CMS-NOTE-2007-024](#) (2007);
P. Biallass and T. Hebbeker, *Parametrization of the Cosmic Muon Flux for the Generator CMSCGEN*, [arXiv:0907.5514](#).
- [10] PARTICLE DATA GROUP collaboration, W.M. Yao et al., *Review of particle physics*, *J. Phys. G* **33** (2006) 1.
- [11] D. Acosta et al., *Measuring Muon Reconstruction Efficiency from Data*, [CMS-NOTE-2006-060](#) (2006);
R. Breedon et al., *Efficiency of finding muon track trigger primitives in CMS cathode strip chambers*, *Nucl. Instrum. Meth. A* **592** (2008) 26.
- [12] V. Barashko et al., *Fast Algorithm for Track Segment and Hit Reconstruction in the CMS Cathode Strip Chambers*, *Nucl. Instrum. Meth. A* **589/3** (2008) 26.
- [13] E. Gatti, A. Longoni, P. Semenza and H. Okuno, *Optimum geometry for strip cathodes or grids in MWPC for avalanche localization along the anode wires*, *Nucl. Instrum. Meth.* **163** (1979) 83.
- [14] E. Mathieson and J. Gordon, *Cathode Charge Distributions in Multiwire Chambers: I. Measurement and Theory*, *Nucl. Instrum. Meth.* **227** (1984) 267;
II. Approximate and Empirical Formulae, *Nucl. Instrum. Meth.* **227** (1984) 277.
- [15] I. Golutvin et al., *Cathode Strip Chambers Data Analysis*, in proceedings of the *Seventh International Conference on Advanced Technology and Particle Physics*, Como, Italy, 15–19 October 2001.
- [16] Yu V. Erchov et al., *Cathode Strip Chamber for CMS ME1/1 Endcap Muon Station*, *Phys. Part. Nucl. Lett.* **3** (2006) 183.

The CMS collaboration

Yerevan Physics Institute, Yerevan, Armenia

S. Chatrchyan, V. Khachatryan, A.M. Sirunyan

Institut für Hochenergiephysik der OeAW, Wien, Austria

W. Adam, B. Arnold, H. Bergauer, T. Bergauer, M. Dragicevic, M. Eichberger, J. Erö, M. Friedl, R. Frühwirth, V.M. Ghete, J. Hammer¹, S. Hänsel, M. Hoch, N. Hörmann, J. Hrubec, M. Jeitler, G. Kasieczka, K. Kastner, M. Krammer, D. Liko, I. Magrans de Abril, I. Mikulec, F. Mittermayr, B. Neuherz, M. Oberegger, M. Padrta, M. Pernicka, H. Rohringer, S. Schmid, R. Schöfbeck, T. Schreiner, R. Stark, H. Steininger, J. Strauss, A. Taurok, F. Teischinger, T. Themel, D. Uhl, P. Wagner, W. Waltenberger, G. Walzel, E. Widl, C.-E. Wulz

National Centre for Particle and High Energy Physics, Minsk, Belarus

V. Chekhovsky, O. Dvornikov, I. Emeliantchik, A. Litomin, V. Makarenko, I. Marfin, V. Mossolov, N. Shumeiko, A. Solin, R. Stefanovitch, J. Suarez Gonzalez, A. Tikhonov

Research Institute for Nuclear Problems, Minsk, Belarus

A. Fedorov, A. Karneyeu, M. Korzhik, V. Panov, R. Zuyevski

Research Institute of Applied Physical Problems, Minsk, Belarus

P. Kuchinsky

Universiteit Antwerpen, Antwerpen, Belgium

W. Beaumont, L. Benucci, M. Cardaci, E.A. De Wolf, E. Delmeire, D. Druzhkin, M. Hashemi, X. Janssen, T. Maes, L. Mucibello, S. Ochesanu, R. Rougny, M. Selvaggi, H. Van Haevermaet, P. Van Mechelen, N. Van Remortel

Vrije Universiteit Brussel, Brussel, Belgium

V. Adler, S. Beauceron, S. Blyweert, J. D'Hondt, S. De Weirdt, O. Devroede, J. Heyninck, A. Kalogeropoulos, J. Maes, M. Maes, M.U. Mozer, S. Tavernier, W. Van Doninck¹, P. Van Mulders, I. Vilella

Université Libre de Bruxelles, Bruxelles, Belgium

O. Bouhali, E.C. Chabert, O. Charaf, B. Clerboux, G. De Lentdecker, V. Dero, S. Elgammal, A.P.R. Gay, G.H. Hammad, P.E. Marage, S. Rugovac, C. Vander Velde, P. Vanlaer, J. Wickens

Ghent University, Ghent, Belgium

M. Grunewald, B. Klein, A. Marinov, D. Ryckbosch, F. Thyssen, M. Tytgat, L. Vanelderen, P. Verwilligen

Université Catholique de Louvain, Louvain-la-Neuve, Belgium

S. Basegmez, G. Bruno, J. Caudron, C. Delaere, P. Demin, D. Favart, A. Giammanco, G. Grégoire, V. Lemaitre, O. Militaru, S. Ovyn, K. Piotrkowski¹, L. Quertenmont, N. Schul

Université de Mons, Mons, Belgium

N. Beliy, E. Daubie

Centro Brasileiro de Pesquisas Fisicas, Rio de Janeiro, Brazil

G.A. Alves, M.E. Pol, M.H.G. Souza

Universidade do Estado do Rio de Janeiro, Rio de Janeiro, Brazil

W. Carvalho, D. De Jesus Damiao, C. De Oliveira Martins, S. Fonseca De Souza, L. Mundim, V. Oguri, A. Santoro, S.M. Silva Do Amaral, A. Sznajder

Instituto de Fisica Teorica, Universidade Estadual Paulista, Sao Paulo, Brazil

T.R. Fernandez Perez Tomei, M.A. Ferreira Dias, E. M. Gregores², S.F. Novaes

Institute for Nuclear Research and Nuclear Energy, Sofia, Bulgaria

K. Abadjiev¹, T. Anguelov, J. Damgov, N. Darmenov¹, L. Dimitrov, V. Genchev¹, P. Iaydjiev, S. Piperov, S. Stoykova, G. Sultanov, R. Trayanov, I. Vankov

University of Sofia, Sofia, Bulgaria

A. Dimitrov, M. Dyulendarova, V. Kozhuharov, L. Litov, E. Marinova, M. Mateev, B. Pavlov, P. Petkov, Z. Toteva¹

Institute of High Energy Physics, Beijing, China

G.M. Chen, H.S. Chen, W. Guan, C.H. Jiang, D. Liang, B. Liu, X. Meng, J. Tao, J. Wang, Z. Wang, Z. Xue, Z. Zhang

State Key Lab. of Nucl. Phys. and Tech., Peking University, Beijing, China

Y. Ban, J. Cai, Y. Ge, S. Guo, Z. Hu, Y. Mao, S.J. Qian, H. Teng, B. Zhu

Universidad de Los Andes, Bogota, Colombia

C. Avila, M. Baquero Ruiz, C.A. Carrillo Montoya, A. Gomez, B. Gomez Moreno, A.A. Ocampo Rios, A.F. Osorio Oliveros, D. Reyes Romero, J.C. Sanabria

Technical University of Split, Split, Croatia

N. Godinovic, K. Lelas, R. Plestina, D. Polic, I. Puljak

University of Split, Split, Croatia

Z. Antunovic, M. Dzelalija

Institute Rudjer Boskovic, Zagreb, Croatia

V. Brigljevic, S. Duric, K. Kadija, S. Morovic

University of Cyprus, Nicosia, Cyprus

R. Fereos, M. Galanti, J. Mousa, A. Papadakis, F. Ptochos, P.A. Razis, D. Tsiakkouri, Z. Zinonos

National Institute of Chemical Physics and Biophysics, Tallinn, Estonia

A. Hektor, M. Kadastik, K. Kannike, M. Müntel, M. Raidal, L. Rebane

Helsinki Institute of Physics, Helsinki, Finland

E. Anttila, S. Czellar, J. Härkönen, A. Heikkinen, V. Karimäki, R. Kinnunen, J. Klem, M.J. Kortelainen, T. Lampén, K. Lassila-Perini, S. Lehti, T. Lindén, P. Luukka, T. Mäenpää, J. Nysten, E. Tuominen, J. Tuominiemi, D. Ungaro, L. Wendland

Lappeenranta University of Technology, Lappeenranta, Finland

K. Banzuzi, A. Korpela, T. Tuuva

Laboratoire d'Annecy-le-Vieux de Physique des Particules, IN2P3-CNRS, Annecy-le-Vieux, France

P. Nedelec, D. Sillou

DSM/IRFU, CEA/Saclay, Gif-sur-Yvette, France

M. Besancon, R. Chipaux, M. Dejardin, D. Denegri, J. Descamps, B. Fabbro, J.L. Faure, F. Ferri, S. Ganjour, F.X. Gentit, A. Givernaud, P. Gras, G. Hamel de Monchenault, P. Jarry, M.C. Lemaire, E. Locci, J. Malcles, M. Marionneau, L. Millischer, J. Rander, A. Rosowsky, D. Rousseau, M. Titov, P. Verrecchia

Laboratoire Leprince-Ringuet, Ecole Polytechnique, IN2P3-CNRS, Palaiseau, France

S. Baffioni, L. Bianchini, M. Bluj³, P. Busson, C. Charlot, L. Dobrzynski, R. Granier de Cassagnac, M. Haguenaue, P. Miné, P. Paganini, Y. Sirois, C. Thiebaux, A. Zabi

Institut Pluridisciplinaire Hubert Curien, Université de Strasbourg, Université de Haute Alsace Mulhouse, CNRS/IN2P3, Strasbourg, France

J.-L. Agram⁴, A. Besson, D. Bloch, D. Bodin, J.-M. Brom, E. Conte⁴, F. Drouhin⁴, J.-C. Fontaine⁴, D. Gelé, U. Goerlach, L. Gross, P. Juillot, A.-C. Le Bihan, Y. Patois, J. Speck, P. Van Hove

Université de Lyon, Université Claude Bernard Lyon 1, CNRS-IN2P3, Institut de Physique Nucléaire de Lyon, Villeurbanne, France

C. Baty, M. Bedjidian, J. Blaha, G. Boudoul, H. Brun, N. Chanon, R. Chierici, D. Contardo, P. Depasse, T. Dupasquier, H. El Mamouni, F. Fassi⁵, J. Fay, S. Gascon, B. Ille, T. Kurca, T. Le Grand, M. Lethuillier, N. Lumb, L. Mirabito, S. Perries, M. Vander Donckt, P. Verdier

E. Andronikashvili Institute of Physics, Academy of Science, Tbilisi, Georgia

N. Djaoshvili, N. Roinishvili, V. Roinishvili

Institute of High Energy Physics and Informatization, Tbilisi State University, Tbilisi, Georgia

N. Amaglobeli

RWTH Aachen University, I. Physikalisches Institut, Aachen, Germany

R. Adolphi, G. Anagnostou, R. Brauer, W. Braunschweig, M. Edelhoff, H. Esser, L. Feld, W. Karpinski, A. Khomich, K. Klein, N. Mohr, A. Ostapchouk, D. Pandoulas, G. Pierschel, F. Raupach, S. Schael, A. Schultz von Dratzig, G. Schwering, D. Sprenger, M. Thomas, M. Weber, B. Wittmer, M. Wlochal

RWTH Aachen University, III. Physikalisches Institut A, Aachen, Germany

O. Actis, G. Altenhöfer, W. Bender, P. Biallass, M. Erdmann, G. Fetchenhauer¹, J. Frangenheim, T. Hebbeker, G. Hilgers, A. Hinzmann, K. Hoepfner, C. Hof, M. Kirsch, T. Klimkovich, P. Kreuzer¹, D. Lanske[†], M. Merschmeyer, A. Meyer, B. Philipps, H. Pieta, H. Reithler, S.A. Schmitz, L. Sonnenschein, M. Sowa, J. Steggemann, H. Szczesny, D. Teyssier, C. Zeidler

RWTH Aachen University, III. Physikalisches Institut B, Aachen, Germany

M. Bontenackels, M. Davids, M. Duda, G. Flügge, H. Geenen, M. Giffels, W. Haj Ahmad, T. Hermanns, D. Heydhausen, S. Kalinin, T. Kress, A. Linn, A. Nowack, L. Perchalla, M. Poettgens, O. Pooth, P. Sauerland, A. Stahl, D. Tornier, M.H. Zoeller

Deutsches Elektronen-Synchrotron, Hamburg, Germany

M. Aldaya Martin, U. Behrens, K. Borras, A. Campbell, E. Castro, D. Dammann, G. Eckerlin, A. Flossdorf, G. Flucke, A. Geiser, D. Hatton, J. Hauk, H. Jung, M. Kasemann, I. Katkov, C. Kleinwort, H. Kluge, A. Knutsson, E. Kuznetsova, W. Lange, W. Lohmann, R. Mankel¹,

M. Marienfeld, A.B. Meyer, S. Miglioranza, J. Mnich, M. Ohlerich, J. Olzem, A. Parenti, C. Rosemann, R. Schmidt, T. Schoerner-Sadenius, D. Volyanskyy, C. Wissing, W.D. Zeuner¹

University of Hamburg, Hamburg, Germany

C. Autermann, F. Bechtel, J. Draeger, D. Eckstein, U. Gebbert, K. Kaschube, G. Kaussen, R. Klanner, B. Mura, S. Naumann-Emme, F. Nowak, U. Pein, C. Sander, P. Schleper, T. Schum, H. Stadie, G. Steinbrück, J. Thomsen, R. Wolf

Institut für Experimentelle Kernphysik, Karlsruhe, Germany

J. Bauer, P. Blüm, V. Buege, A. Cakir, T. Chwalek, W. De Boer, A. Dierlamm, G. Dirkes, M. Feindt, U. Felzmann, M. Frey, A. Furgeri, J. Gruschke, C. Hackstein, F. Hartmann¹, S. Heier, M. Heinrich, H. Held, D. Hirschbuehl, K.H. Hoffmann, S. Honc, C. Jung, T. Kuhr, T. Liamsuwan, D. Martschei, S. Mueller, Th. Müller, M.B. Neuland, M. Niegel, O. Oberst, A. Oehler, J. Ott, T. Peiffer, D. Piparo, G. Quast, K. Rabbertz, F. Ratnikov, N. Ratnikova, M. Renz, C. Saout¹, G. Sartisoehn, A. Scheurer, P. Schieferdecker, F.-P. Schilling, G. Schott, H.J. Simonis, F.M. Stober, P. Sturm, D. Troendle, A. Trunov, W. Wagner, J. Wagner-Kuhr, M. Zeise, V. Zhukov⁶, E.B. Ziebarth

Institute of Nuclear Physics "Demokritos", Aghia Paraskevi, Greece

G. Daskalakis, T. Geralis, K. Karafasoulis, A. Kyriakis, D. Loukas, A. Markou, C. Markou, C. Mavrommatis, E. Petrakou, A. Zachariadou

University of Athens, Athens, Greece

L. Gouskos, P. Katsas, A. Panagiotou¹

University of Ioánnina, Ioánnina, Greece

I. Evangelou, P. Kokkas, N. Manthos, I. Papadopoulos, V. Patras, F.A. Triantis

KFKI Research Institute for Particle and Nuclear Physics, Budapest, Hungary

G. Bencze¹, L. Boldizsar, G. Debreczeni, C. Hajdu¹, S. Hernath, P. Hidas, D. Horvath⁷, K. Krajczar, A. Laszlo, G. Patay, F. Sikler, N. Toth, G. Vesztergombi

Institute of Nuclear Research ATOMKI, Debrecen, Hungary

N. Beni, G. Christian, J. Imrek, J. Molnar, D. Novak, J. Palinkas, G. Szekely, Z. Szillasi¹, K. Tokesi, V. Veszpremi

University of Debrecen, Debrecen, Hungary

A. Kapusi, G. Marian, P. Raics, Z. Szabo, Z.L. Trocsanyi, B. Ujvari, G. Zilizi

Panjab University, Chandigarh, India

S. Bansal, H.S. Bawa, S.B. Beri, V. Bhatnagar, M. Jindal, M. Kaur, R. Kaur, J.M. Kohli, M.Z. Mehta, N. Nishu, L.K. Saini, A. Sharma, A. Singh, J.B. Singh, S.P. Singh

University of Delhi, Delhi, India

S. Ahuja, S. Arora, S. Bhattacharya⁸, S. Chauhan, B.C. Choudhary, P. Gupta, S. Jain, S. Jain, M. Jha, A. Kumar, K. Ranjan, R.K. Shivpuri, A.K. Srivastava

Bhabha Atomic Research Centre, Mumbai, India

R.K. Choudhury, D. Dutta, S. Kailas, S.K. Kataria, A.K. Mohanty, L.M. Pant, P. Shukla, A. Topkar

Tata Institute of Fundamental Research - EHEP, Mumbai, India

T. Aziz, M. Guchait⁹, A. Gurtu, M. Maity¹⁰, D. Majumder, G. Majumder, K. Mazumdar, A. Nayak, A. Saha, K. Sudhakar

Tata Institute of Fundamental Research - HECR, Mumbai, India

S. Banerjee, S. Dugad, N.K. Mondal

Institute for Studies in Theoretical Physics & Mathematics (IPM), Tehran, Iran

H. Arfaei, H. Bakhshiansohi, A. Fahim, A. Jafari, M. Mohammadi Najafabadi, A. Moshaii, S. Paktinat Mehdiabadi, S. Rouhani, B. Safarzadeh, M. Zeinali

University College Dublin, Dublin, Ireland

M. Felcini

INFN Sezione di Bari ^a, Università di Bari ^b, Politecnico di Bari ^c, Bari, Italy

M. Abbrescia^{a,b}, L. Barbone^a, F. Chiumarulo^a, A. Clemente^a, A. Colaleo^a, D. Creanza^{a,c}, G. Cuscela^a, N. De Filippis^a, M. De Palma^{a,b}, G. De Robertis^a, G. Donvito^a, F. Fedele^a, L. Fiore^a, M. Franco^a, G. Iaselli^{a,c}, N. Lacalamita^a, F. Loddo^a, L. Lusito^{a,b}, G. Maggi^{a,c}, M. Maggi^a, N. Manna^{a,b}, B. Marangelli^{a,b}, S. My^{a,c}, S. Natali^{a,b}, S. Nuzzo^{a,b}, G. Papagni^a, S. Piccolomo^a, G.A. Pierro^a, C. Pinto^a, A. Pompili^{a,b}, G. Pugliese^{a,c}, R. Rajan^a, A. Ranieri^a, F. Romano^{a,c}, G. Roselli^{a,b}, G. Selvaggi^{a,b}, Y. Shinde^a, L. Silvestris^a, S. Tupputi^{a,b}, G. Zito^a

INFN Sezione di Bologna ^a, Università di Bologna ^b, Bologna, Italy

G. Abbiendi^a, W. Bacchi^{a,b}, A.C. Benvenuti^a, M. Boldini^a, D. Bonacorsi^a, S. Braibant-Giacomelli^{a,b}, V.D. Cafaro^a, S.S. Caiazza^a, P. Capiluppi^{a,b}, A. Castro^{a,b}, F.R. Cavallo^a, G. Codispoti^{a,b}, M. Cuffiani^{a,b}, I. D'Antone^a, G.M. Dallavalle^{a,1}, F. Fabbri^a, A. Fanfani^{a,b}, D. Fasanella^a, P. Giacomelli^a, V. Giordano^a, M. Giunta^{a,1}, C. Grandi^a, M. Guerzoni^a, S. Marcellini^a, G. Masetti^{a,b}, A. Montanari^a, F.L. Navarria^{a,b}, F. Odorici^a, G. Pellegrini^a, A. Perrotta^a, A.M. Rossi^{a,b}, T. Rovelli^{a,b}, G. Siroli^{a,b}, G. Torromeo^a, R. Travaglini^{a,b}

INFN Sezione di Catania ^a, Università di Catania ^b, Catania, Italy

S. Albergo^{a,b}, S. Costa^{a,b}, R. Potenza^{a,b}, A. Tricomi^{a,b}, C. Tuve^a

INFN Sezione di Firenze ^a, Università di Firenze ^b, Firenze, Italy

G. Barbagli^a, G. Broccolo^{a,b}, V. Ciulli^{a,b}, C. Civinini^a, R. D'Alessandro^{a,b}, E. Focardi^{a,b}, S. Frosali^{a,b}, E. Gallo^a, C. Genta^{a,b}, G. Landi^{a,b}, P. Lenzi^{a,b,1}, M. Meschini^a, S. Paoletti^a, G. Sguazzoni^a, A. Tropiano^a

INFN Laboratori Nazionali di Frascati, Frascati, Italy

L. Benussi, M. Bertani, S. Bianco, S. Colafranceschi¹¹, D. Colonna¹¹, F. Fabbri, M. Giardoni, L. Passamonti, D. Piccolo, D. Pierluigi, B. Ponzio, A. Russo

INFN Sezione di Genova, Genova, Italy

P. Fabbricatore, R. Musenich

INFN Sezione di Milano-Bicocca ^a, Università di Milano-Bicocca ^b, Milano, Italy

A. Benaglia^a, M. Calloni^a, G.B. Cerati^{a,b,1}, P. D'Angelo^a, F. De Guio^a, F.M. Farina^a, A. Ghezzi^a, P. Govoni^{a,b}, M. Malberti^{a,b,1}, S. Malvezzi^a, A. Martelli^a, D. Menasce^a, V. Miccio^{a,b}, L. Moroni^a, P. Negri^{a,b}, M. Paganoni^{a,b}, D. Pedrini^a, A. Pullia^{a,b}, S. Ragazzi^{a,b}, N. Redaelli^a, S. Sala^a, R. Salerno^{a,b}, T. Tabarelli de Fatis^{a,b}, V. Tancini^{a,b}, S. Taroni^{a,b}

INFN Sezione di Napoli ^a, Università di Napoli "Federico II" ^b, Napoli, Italy

S. Buontempo^a, N. Cavallo^a, A. Cimmino^{a,b,1}, M. De Gruttola^{a,b,1}, F. Fabozzi^{a,12}, A.O.M. Iorio^a, L. Lista^a, D. Lomidze^a, P. Noli^{a,b}, P. Paolucci^a, C. Sciacca^{a,b}

INFN Sezione di Padova ^a, Università di Padova ^b, Padova, Italy

P. Azzi^{a,1}, N. Bacchetta^a, L. Barcellan^a, P. Bellan^{a,b,1}, M. Bellato^a, M. Benettoni^a, M. Biasotto^{a,13}, D. Bisello^{a,b}, E. Borsato^{a,b}, A. Branca^a, R. Carlin^{a,b}, L. Castellani^a, P. Checchia^a, E. Conti^a, F. Dal Corso^a, M. De Mattia^{a,b}, T. Dorigo^a, U. Dosselli^a, F. Fanzago^a, F. Gasparini^{a,b}, U. Gasparini^{a,b}, P. Giubilato^{a,b}, F. Gonella^a, A. Gresele^{a,14}, M. Gulmini^{a,13}, A. Kaminskiy^{a,b}, S. Lacaprara^{a,13}, I. Lazzizzera^{a,14}, M. Margoni^{a,b}, G. Maron^{a,13}, S. Mattiazzo^{a,b}, M. Mazzucato^a, M. Meneghelli^a, A.T. Meneguzzo^{a,b}, M. Michelotto^a, F. Montecassiano^a, M. Nespolo^a, M. Passaseo^a, M. Pegoraro^a, L. Perrozzi^a, N. Pozzobon^{a,b}, P. Ronchese^{a,b}, F. Simonetto^{a,b}, N. Toniolo^a, E. Torassa^a, M. Tosi^{a,b}, A. Triossi^a, S. Vanini^{a,b}, S. Ventura^a, P. Zotto^{a,b}, G. Zumerle^{a,b}

INFN Sezione di Pavia ^a, Università di Pavia ^b, Pavia, Italy

P. Baesso^{a,b}, U. Berzano^a, S. Bricola^a, M.M. Necchi^{a,b}, D. Pagano^{a,b}, S.P. Ratti^{a,b}, C. Riccardi^{a,b}, P. Torre^{a,b}, A. Vicini^a, P. Vitulo^{a,b}, C. Viviani^{a,b}

INFN Sezione di Perugia ^a, Università di Perugia ^b, Perugia, Italy

D. Aisa^a, S. Aisa^a, E. Babucci^a, M. Biasini^{a,b}, G.M. Bilei^a, B. Caponeri^{a,b}, B. Checcucci^a, N. Dinu^a, L. Fanò^a, L. Farnesini^a, P. Lariccia^{a,b}, A. Lucaroni^{a,b}, G. Mantovani^{a,b}, A. Nappi^{a,b}, A. Piluso^a, V. Postolache^a, A. Santocchia^{a,b}, L. Servoli^a, D. Tonoiu^a, A. Vedae^a, R. Volpe^{a,b}

INFN Sezione di Pisa ^a, Università di Pisa ^b, Scuola Normale Superiore di Pisa ^c, Pisa, Italy

P. Azzurri^{a,c}, G. Bagliesi^a, J. Bernardini^{a,b}, L. Berretta^a, T. Boccali^a, A. Bocci^{a,c}, L. Borrello^{a,c}, F. Bosi^a, F. Calzolari^a, R. Castaldi^a, R. Dell'Orso^a, F. Fiori^{a,b}, L. Foà^{a,c}, S. Gennai^{a,c}, A. Giassi^a, A. Kraan^a, F. Ligabue^{a,c}, T. Lomtadze^a, F. Mariani^a, L. Martini^a, M. Massa^a, A. Messineo^{a,b}, A. Moggi^a, F. Palla^a, F. Palmonari^a, G. Petraghani^a, G. Petrucciani^{a,c}, F. Raffaelli^a, S. Sarkar^a, G. Segneri^a, A.T. Serban^a, P. Spagnolo^{a,1}, R. Tenchini^{a,1}, S. Tolaini^a, G. Tonelli^{a,b,1}, A. Venturi^a, P.G. Verdini^a

INFN Sezione di Roma ^a, Università di Roma "La Sapienza" ^b, Roma, Italy

S. Baccaro^{a,15}, L. Barone^{a,b}, A. Bartoloni^a, F. Cavallari^{a,1}, I. Dafinei^a, D. Del Re^{a,b}, E. Di Marco^{a,b}, M. Diemoz^a, D. Franci^{a,b}, E. Longo^{a,b}, G. Organtini^{a,b}, A. Palma^{a,b}, F. Pandolfi^{a,b}, R. Paramatti^{a,1}, F. Pellegrino^a, S. Rahatlou^{a,b}, C. Rovelli^a

INFN Sezione di Torino ^a, Università di Torino ^b, Università del Piemonte Orientale (Novara) ^c, Torino, Italy

G. Alampi^a, N. Amapane^{a,b}, R. Arcidiacono^{a,b}, S. Argiro^{a,b}, M. Arneodo^{a,c}, C. Biino^a, M.A. Borgia^{a,b}, C. Botta^{a,b}, N. Cartiglia^a, R. Castello^{a,b}, G. Cerminara^{a,b}, M. Costa^{a,b}, D. Dattola^a, G. Dellacasa^a, N. Demaria^a, G. Dughera^a, F. Dumitrache^a, A. Graziano^{a,b}, C. Mariotti^a, M. Marone^{a,b}, S. Maselli^a, E. Migliore^{a,b}, G. Mila^{a,b}, V. Monaco^{a,b}, M. Musich^{a,b}, M. Nervo^{a,b}, M.M. Obertino^{a,c}, S. Oggero^{a,b}, R. Panero^a, N. Pastrone^a, M. Pelliccioni^{a,b}, A. Romero^{a,b}, M. Ruspa^{a,c}, R. Sacchi^{a,b}, A. Solano^{a,b}, A. Staiano^a, P.P. Trapani^{a,b,1}, D. Trocino^{a,b}, A. Vilela Pereira^{a,b}, L. Visca^{a,b}, A. Zampieri^a

INFN Sezione di Trieste ^a, Università di Trieste ^b, Trieste, Italy

F. Ambroglini^{a,b}, S. Belforte^a, F. Cossutti^a, G. Della Ricca^{a,b}, B. Gobbo^a, A. Penzo^a

Kyungpook National University, Daegu, Korea

S. Chang, J. Chung, D.H. Kim, G.N. Kim, D.J. Kong, H. Park, D.C. Son

Wonkwang University, Iksan, Korea

S.Y. Bahk

Chonnam National University, Kwangju, Korea

S. Song

Konkuk University, Seoul, Korea

S.Y. Jung

Korea University, Seoul, Korea

B. Hong, H. Kim, J.H. Kim, K.S. Lee, D.H. Moon, S.K. Park, H.B. Rhee, K.S. Sim

Seoul National University, Seoul, Korea

J. Kim

University of Seoul, Seoul, Korea

M. Choi, G. Hahn, I.C. Park

Sungkyunkwan University, Suwon, Korea

S. Choi, Y. Choi, J. Goh, H. Jeong, T.J. Kim, J. Lee, S. Lee

Vilnius University, Vilnius, Lithuania

M. Janulis, D. Martisiute, P. Petrov, T. Sabonis

Centro de Investigacion y de Estudios Avanzados del IPN, Mexico City, MexicoH. Castilla Valdez¹, A. Sánchez Hernández**Universidad Iberoamericana, Mexico City, Mexico**

S. Carrillo Moreno

Universidad Autónoma de San Luis Potosí, San Luis Potosí, Mexico

A. Morelos Pineda

University of Auckland, Auckland, New Zealand

P. Allfrey, R.N.C. Gray, D. Krofcheck

University of Canterbury, Christchurch, New Zealand

N. Bernardino Rodrigues, P.H. Butler, T. Signal, J.C. Williams

National Centre for Physics, Quaid-I-Azam University, Islamabad, Pakistan

M. Ahmad, I. Ahmed, W. Ahmed, M.I. Asghar, M.I.M. Awan, H.R. Hoorani, I. Hussain, W.A. Khan, T. Khurshid, S. Muhammad, S. Qazi, H. Shahzad

Institute of Experimental Physics, Warsaw, PolandM. Cwiok, R. Dabrowski, W. Dominik, K. Doroba, M. Konecki, J. Krolikowski, K. Pozniak¹⁶, R. Romaniuk, W. Zabolotny¹⁶, P. Zych**Soltan Institute for Nuclear Studies, Warsaw, Poland**

T. Frueboes, R. Gokieli, L. Gosciolo, M. Górski, M. Kazana, K. Nawrocki, M. Szleper, G. Wrochna, P. Zalewski

Laboratório de Instrumentação e Física Experimental de Partículas, Lisboa, Portugal

N. Almeida, L. Antunes Pedro, P. Bargassa, A. David, P. Faccioli, P.G. Ferreira Parracho, M. Freitas Ferreira, M. Gallinaro, M. Guerra Jordao, P. Martins, G. Mini, P. Musella, J. Pela, L. Raposo, P.Q. Ribeiro, S. Sampaio, J. Seixas, J. Silva, P. Silva, D. Soares, M. Sousa, J. Varela, H.K. Wöhri

Joint Institute for Nuclear Research, Dubna, Russia

I. Altsybeev, I. Belotelov, P. Bunin, Y. Ershov, I. Filozova, M. Finger, M. Finger Jr., A. Golunov, I. Golutvin, N. Gorbounov, V. Kalagin, A. Kamenev, V. Karjavin, V. Konoplyanikov, V. Korenkov, G. Kozlov, A. Kurenkov, A. Lanev, A. Makankin, V.V. Mitsyn, P. Moisezenz, E. Nikonov, D. Oleynik, V. Palichik, V. Perelygin, A. Petrosyan, R. Semenov, S. Shmatov, V. Smirnov, D. Smolin, E. Tikhonenko, S. Vasil'ev, A. Vishnevskiy, A. Volodko, A. Zarubin, V. Zhiltsov

Petersburg Nuclear Physics Institute, Gatchina (St Petersburg), Russia

N. Bondar, L. Chtchipounov, A. Denisov, Y. Gavrikov, G. Gavrilov, V. Golovtsov, Y. Ivanov, V. Kim, V. Kozlov, P. Levchenko, G. Obrant, E. Orishchin, A. Petrunin, Y. Shcheglov, A. Shchetkovskiy, V. Sknar, I. Smirnov, V. Sulimov, V. Tarakanov, L. Uvarov, S. Vavilov, G. Velichko, S. Volkov, A. Vorobyev

Institute for Nuclear Research, Moscow, Russia

Yu. Andreev, A. Anisimov, P. Antipov, A. Dermenev, S. Gninenko, N. Golubev, M. Kirsanov, N. Krasnikov, V. Matveev, A. Pashenkov, V.E. Postoev, A. Solovey, A. Solovey, A. Toropin, S. Troitsky

Institute for Theoretical and Experimental Physics, Moscow, Russia

A. Baud, V. Epshteyn, V. Gavrilov, N. Ilina, V. Kaftanov[†], V. Kolosov, M. Kossov¹, A. Krokhotin, S. Kuleshov, A. Oulianov, G. Safronov, S. Semenov, I. Shreyber, V. Stolin, E. Vlasov, A. Zhokin

Moscow State University, Moscow, Russia

E. Boos, M. Dubinin¹⁷, L. Dudko, A. Ershov, A. Gribushin, V. Klyukhin, O. Kodolova, I. Lokhtin, S. Petrushanko, L. Sarycheva, V. Savrin, A. Snigirev, I. Vardanyan

P.N. Lebedev Physical Institute, Moscow, Russia

I. Dremin, M. Kirakosyan, N. Konovalova, S.V. Rusakov, A. Vinogradov

State Research Center of Russian Federation, Institute for High Energy Physics, Protvino, Russia

S. Akimenko, A. Artamonov, I. Azhgirey, S. Bitioukov, V. Burtovoy, V. Grishin¹, V. Kachanov, D. Konstantinov, V. Krychkin, A. Levine, I. Lobov, V. Lukanin, Y. Mel'nik, V. Petrov, R. Ryutin, S. Slabospitsky, A. Sobol, A. Sytine, L. Tourtchanovitch, S. Troshin, N. Tyurin, A. Uzunian, A. Volkov

Vinca Institute of Nuclear Sciences, Belgrade, Serbia

P. Adzic, M. Djordjevic, D. Jovanovic¹⁸, D. Krpic¹⁸, D. Maletic, J. Puzovic¹⁸, N. Smiljkovic

Centro de Investigaciones Energéticas Medioambientales y Tecnológicas (CIEMAT), Madrid, Spain

M. Aguilar-Benitez, J. Alberdi, J. Alcaraz Maestre, P. Arce, J.M. Barcala, C. Battilana, C. Burgos Lazaro, J. Caballero Bejar, E. Calvo, M. Cardenas Montes, M. Cepeda, M. Cerrada, M. Chamizo Llatas, F. Clemente, N. Colino, M. Daniel, B. De La Cruz, A. Delgado Peris, C. Diez Pardos, C. Fernandez Bedoya, J.P. Fernández Ramos, A. Ferrando, J. Flix, M.C. Fouz, P. Garcia-Abia, A.C. Garcia-Bonilla, O. Gonzalez Lopez, S. Goy Lopez, J.M. Hernandez, M.I. Josa, J. Marin, G. Merino, J. Molina, A. Molinero, J.J. Navarrete, J.C. Oller, J. Puerta Pelayo, L. Romero, J. Santaolalla, C. Villanueva Munoz, C. Willmott, C. Yuste

Universidad Autónoma de Madrid, Madrid, Spain

C. Albajar, M. Blanco Otano, J.F. de Trocóniz, A. García Raboso, J.O. Lopez Berengueres

Universidad de Oviedo, Oviedo, Spain

J. Cuevas, J. Fernandez Menendez, I. Gonzalez Caballero, L. Lloret Iglesias, H. Naves Sordo, J.M. Vizan Garcia

Instituto de Física de Cantabria (IFCA), CSIC-Universidad de Cantabria, Santander, Spain

I.J. Cabrillo, A. Calderon, S.H. Chuang, I. Diaz Merino, C. Diez Gonzalez, J. Duarte Campderros, M. Fernandez, G. Gomez, J. Gonzalez Sanchez, R. Gonzalez Suarez, C. Jorda, P. Lobelle Pardo, A. Lopez Virto, J. Marco, R. Marco, C. Martinez Rivero, P. Martinez Ruiz del Arbol, F. Matorras, T. Rodrigo, A. Ruiz Jimeno, L. Scodellaro, M. Sobron Sanudo, I. Vila, R. Vilar Cortabitarte

CERN, European Organization for Nuclear Research, Geneva, Switzerland

D. Abbaneo, E. Albert, M. Alidra, S. Ashby, E. Auffray, J. Baechler, P. Baillon, A.H. Ball, S.L. Bally, D. Barney, F. Beaudette¹⁹, R. Bellan, D. Benedetti, G. Benelli, C. Bernet, P. Bloch, S. Bolognesi, M. Bona, J. Bos, N. Bourgeois, T. Bourrel, H. Breuker, K. Bunkowski, D. Campi, T. Camporesi, E. Cano, A. Cattai, J.P. Chatelain, M. Chauvey, T. Christiansen, J.A. Coarasa Perez, A. Conde Garcia, R. Covarelli, B. Curé, A. De Roeck, V. Delachenal, D. Deyrail, S. Di Vincenzo²⁰, S. Dos Santos, T. Dupont, L.M. Edera, A. Elliott-Peisert, M. Eppard, M. Favre, N. Frank, W. Funk, A. Gaddi, M. Gastal, M. Gateau, H. Gerwig, D. Gigi, K. Gill, D. Giordano, J.P. Girod, F. Glege, R. Gomez-Reino Garrido, R. Goudard, S. Gowdy, R. Guida, L. Guiducci, J. Gutleber, M. Hansen, C. Hartl, J. Harvey, B. Hegner, H.F. Hoffmann, A. Holzner, A. Honma, M. Huhtinen, V. Innocente, P. Janot, G. Le Godec, P. Lecoq, C. Leonidopoulos, R. Loos, C. Lourenço, A. Lyonnet, A. Macpherson, N. Magini, J.D. Maillefaud, G. Maire, T. Mäki, L. Malgeri, M. Mannelli, L. Masetti, F. Meijers, P. Meridiani, S. Mersi, E. Meschi, A. Meynet Cordonnier, R. Moser, M. Mulders, J. Mulon, M. Noy, A. Oh, G. Olesen, A. Onnela, T. Orimoto, L. Orsini, E. Perez, G. Perinic, J.F. Pernot, P. Petagna, P. Petiot, A. Petrilli, A. Pfeiffer, M. Pierini, M. Pimiä, R. Pintus, B. Pirollet, H. Postema, A. Racz, S. Ravat, S.B. Rew, J. Rodrigues Antunes, G. Rolandi²¹, M. Rovere, V. Ryjov, H. Sakulin, D. Samyn, H. Sauce, C. Schäfer, W.D. Schlatter, M. Schröder, C. Schwick, A. Sciaba, I. Segoni, A. Sharma, N. Siegrist, P. Siegrist, N. Sinanis, T. Sobrier, P. Sphicas²², D. Spiga, M. Spiropulu¹⁷, F. Stöckli, P. Traczyk, P. Tropea, J. Troska, A. Tsirou, L. Veillet, G.I. Veres, M. Voutilainen, P. Wertelaers, M. Zanetti

Paul Scherrer Institut, Villigen, Switzerland

W. Bertl, K. Deiters, W. Erdmann, K. Gabathuler, R. Horisberger, Q. Ingram, H.C. Kaestli, S. König, D. Kotlinski, U. Langenegger, F. Meier, D. Renker, T. Rohe, J. Sibille²³, A. Starodumov²⁴

Institute for Particle Physics, ETH Zurich, Zurich, Switzerland

B. Betev, L. Caminada²⁵, Z. Chen, S. Cittolin, D.R. Da Silva Di Calafiori, S. Dambach²⁵, G. Dissertori, M. Dittmar, C. Eggel²⁵, J. Eugster, G. Faber, K. Freudenreich, C. Grab, A. Hervé, W. Hintz, P. Lecomte, P.D. Luckey, W. Lustermann, C. Marchica²⁵, P. Milenovic²⁶, F. Moortgat, A. Nardulli, F. Nessi-Tedaldi, L. Pape, F. Pauss, T. Punz, A. Rizzi, F.J. Ronga, L. Sala, A.K. Sanchez, M.-C. Sawley, V. Sordini, B. Stieger, L. Tauscher[†], A. Thea, K. Theofilatos, D. Treille, P. Trüb²⁵, M. Weber, L. Wehrli, J. Weng, S. Zelepoukine²⁷

Universität Zürich, Zurich, Switzerland

C. Amsler, V. Chiochia, S. De Visscher, C. Regenfus, P. Robmann, T. Rommerskirchen, A. Schmidt, D. Tsirigkas, L. Wilke

National Central University, Chung-Li, Taiwan

Y.H. Chang, E.A. Chen, W.T. Chen, A. Go, C.M. Kuo, S.W. Li, W. Lin

National Taiwan University (NTU), Taipei, Taiwan

P. Bartalini, P. Chang, Y. Chao, K.F. Chen, W.-S. Hou, Y. Hsiung, Y.J. Lei, S.W. Lin, R.-S. Lu, J. Schümann, J.G. Shiu, Y.M. Tzeng, K. Ueno, Y. Velikzhanin, C.C. Wang, M. Wang

Cukurova University, Adana, Turkey

A. Adiguzel, A. Ayhan, A. Azman Gokce, M.N. Bakirci, S. Cerci, I. Dumanoglu, E. Eskut, S. Girgis, E. Gurpinar, I. Hos, T. Karaman, T. Karaman, A. Kayis Topaksu, P. Kurt, G. Önengüt, G. Önengüt Gökbulut, K. Ozdemir, S. Ozturk, A. Polatöz, K. Sogut²⁸, B. Tali, H. Topakli, D. Uzun, L.N. Vergili, M. Vergili

Middle East Technical University, Physics Department, Ankara, Turkey

I.V. Akin, T. Aliev, S. Bilmis, M. Deniz, H. Gamsizkan, A.M. Guler, K. Öcalan, M. Serin, R. Sever, U.E. Surat, M. Zeyrek

Bogaçi University, Department of Physics, Istanbul, Turkey

M. Deliomeroglu, D. Demir²⁹, E. Gülmez, A. Halu, B. Isildak, M. Kaya³⁰, O. Kaya³⁰, S. Ozkorucuklu³¹, N. Sonmez³²

National Scientific Center, Kharkov Institute of Physics and Technology, Kharkov, Ukraine

L. Levchuk, S. Lukyanenko, D. Soroka, S. Zub

University of Bristol, Bristol, United Kingdom

F. Bostock, J.J. Brooke, T.L. Cheng, D. Cussans, R. Frazier, J. Goldstein, N. Grant, M. Hansen, G.P. Heath, H.F. Heath, C. Hill, B. Huckvale, J. Jackson, C.K. Mackay, S. Metson, D.M. Newbold³³, K. Nirunpong, V.J. Smith, J. Velthuis, R. Walton

Rutherford Appleton Laboratory, Didcot, United Kingdom

K.W. Bell, C. Brew, R.M. Brown, B. Camanzi, D.J.A. Cockerill, J.A. Coughlan, N.I. Geddes, K. Harder, S. Harper, B.W. Kennedy, P. Murray, C.H. Shepherd-Themistocleous, I.R. Tomalin, J.H. Williams[†], W.J. Womersley, S.D. Worm

Imperial College, University of London, London, United Kingdom

R. Bainbridge, G. Ball, J. Ballin, R. Beuselinck, O. Buchmuller, D. Colling, N. Cripps, G. Davies, M. Della Negra, C. Foudas, J. Fulcher, D. Futyan, G. Hall, J. Hays, G. Iles, G. Karapostoli, B.C. MacEvoy, A.-M. Magnan, J. Marrouche, J. Nash, A. Nikitenko²⁴, A. Papageorgiou, M. Pesaresi, K. Petridis, M. Pioppi³⁴, D.M. Raymond, N. Rompotis, A. Rose, M.J. Ryan, C. Seez, P. Sharp, G. Sidiropoulos¹, M. Stettler, M. Stoye, M. Takahashi, A. Tapper, C. Timlin, S. Tourneur, M. Vazquez Acosta, T. Virdee¹, S. Wakefield, D. Wardrope, T. Whyntie, M. Wingham

Brunel University, Uxbridge, United Kingdom

J.E. Cole, I. Goitom, P.R. Hobson, A. Khan, P. Kyberd, D. Leslie, C. Munro, I.D. Reid, C. Siamitros, R. Taylor, L. Teodorescu, I. Yaselli

Boston University, Boston, U.S.A.

T. Bose, M. Carleton, E. Hazen, A.H. Heering, A. Heister, J. St. John, P. Lawson, D. Lazic, D. Osborne, J. Rohlf, L. Sulak, S. Wu

Brown University, Providence, U.S.A.

J. Andrea, A. Avetisyan, S. Bhattacharya, J.P. Chou, D. Cutts, S. Esen, G. Kukartsev, G. Landsberg, M. Narain, D. Nguyen, T. Speer, K.V. Tsang

University of California, Davis, Davis, U.S.A.

R. Breedon, M. Calderon De La Barca Sanchez, M. Case, D. Cebra, M. Chertok, J. Conway, P.T. Cox, J. Dolen, R. Erbacher, E. Friis, W. Ko, A. Kopecky, R. Lander, A. Lister, H. Liu, S. Maruyama, T. Miceli, M. Nikolic, D. Pellett, J. Robles, M. Searle, J. Smith, M. Squires, J. Stilley, M. Tripathi, R. Vasquez Sierra, C. Veelken

University of California, Los Angeles, Los Angeles, U.S.A.

V. Andreev, K. Arisaka, D. Cline, R. Cousins, S. Erhan¹, J. Hauser, M. Ignatenko, C. Jarvis, J. Mumford, C. Plager, G. Rakness, P. Schlein[†], J. Tucker, V. Valuev, R. Wallny, X. Yang

University of California, Riverside, Riverside, U.S.A.

J. Babb, M. Bose, A. Chandra, R. Clare, J.A. Ellison, J.W. Gary, G. Hanson, G.Y. Jeng, S.C. Kao, F. Liu, H. Liu, A. Luthra, H. Nguyen, G. Pasztor³⁵, A. Satpathy, B.C. Shen[†], R. Stringer, J. Sturdy, V. Sytnik, R. Wilken, S. Wimpenny

University of California, San Diego, La Jolla, U.S.A.

J.G. Branson, E. Dusinger, D. Evans, F. Golf, R. Kelley, M. Lebourgeois, J. Letts, E. Lipeles, B. Mangano, J. Muelmenstaedt, M. Norman, S. Padhi, A. Petrucci, H. Pi, M. Pieri, R. Ranieri, M. Sani, V. Sharma, S. Simon, F. Würthwein, A. Yagil

University of California, Santa Barbara, Santa Barbara, U.S.A.

C. Campagnari, M. D'Alfonso, T. Danielson, J. Garberson, J. Incandela, C. Justus, P. Kalavase, S.A. Koay, D. Kovalskyi, V. Krutelyov, J. Lamb, S. Lowette, V. Pavlunin, F. Rebassoo, J. Ribnik, J. Richman, R. Rossin, D. Stuart, W. To, J.R. Vlimant, M. Witherell

California Institute of Technology, Pasadena, U.S.A.

A. Apresyan, A. Bornheim, J. Bunn, M. Chiorboli, M. Gataullin, D. Kcira, V. Litvine, Y. Ma, H.B. Newman, C. Rogan, V. Timciuc, J. Veverka, R. Wilkinson, Y. Yang, L. Zhang, K. Zhu, R.Y. Zhu

Carnegie Mellon University, Pittsburgh, U.S.A.

B. Akgun, R. Carroll, T. Ferguson, D.W. Jang, S.Y. Jun, M. Paulini, J. Russ, N. Terentyev, H. Vogel, I. Vorobiev

University of Colorado at Boulder, Boulder, U.S.A.

J.P. Cumalat, M.E. Dinardo, B.R. Drell, W.T. Ford, B. Heyburn, E. Luiggi Lopez, U. Nauenberg, K. Stenson, K. Ulmer, S.R. Wagner, S.L. Zang

Cornell University, Ithaca, U.S.A.

L. Agostino, J. Alexander, F. Blekman, D. Cassel, A. Chatterjee, S. Das, L.K. Gibbons, B. Heltsley, W. Hopkins, A. Khukhunaishvili, B. Kreis, V. Kuznetsov, J.R. Patterson, D. Puigh, A. Ryd, X. Shi, S. Stroiney, W. Sun, W.D. Teo, J. Thom, J. Vaughan, Y. Weng, P. Wittich

Fairfield University, Fairfield, U.S.A.

C.P. Beetz, G. Cirino, C. Sanzeni, D. Winn

Fermi National Accelerator Laboratory, Batavia, U.S.A.

S. Abdullin, M.A. Afaq¹, M. Albrow, B. Ananthan, G. Apollinari, M. Atac, W. Badgett, L. Bagby, J.A. Bakken, B. Baldin, S. Banerjee, K. Banicz, L.A.T. Bauerdick, A. Beretvas, J. Berryhill, P.C. Bhat, K. Biery, M. Binkley, I. Bloch, F. Borcharding, A.M. Brett, K. Burkett, J.N. Butler, V. Chetluru, H.W.K. Cheung, F. Chlebana, I. Churin, S. Cihangir, M. Crawford, W. Dagenhart, M. Demarteau, G. Derylo, D. Dykstra, D.P. Eartly, J.E. Elias, V.D. Elvira, D. Evans, L. Feng, M. Fischler, I. Fisk, S. Foulkes, J. Freeman, P. Gartung, E. Gottschalk, T. Grassi, D. Green, Y. Guo, O. Gutsche, A. Hahn, J. Hanlon, R.M. Harris, B. Holzman, J. Howell, D. Hufnagel, E. James, H. Jensen, M. Johnson, C.D. Jones, U. Joshi, E. Juska, J. Kaiser, B. Klima, S. Kossiakov, K. Kousouris, S. Kwan, C.M. Lei, P. Limon, J.A. Lopez Perez, S. Los, L. Lueking, G. Lukhanin, S. Lusin¹, J. Lykken, K. Maeshima, J.M. Marraffino, D. Mason, P. McBride, T. Miao, K. Mishra, S. Moccia, R. Mommsen, S. Mrenna, A.S. Muhammad, C. Newman-Holmes, C. Noeding, V. O'Dell, O. Prokofyev, R. Rivera, C.H. Rivetta, A. Ronzhin, P. Rossman, S. Ryu, V. Sekhri, E. Sexton-Kennedy, I. Sfiligoi, S. Sharma, T.M. Shaw, D. Shpakov, E. Skup, R.P. Smith[†], A. Soha, W.J. Spalding, L. Spiegel, I. Suzuki, P. Tan, W. Tanenbaum, S. Tkaczyk¹, R. Trentadue¹, L. Uplegger, E.W. Vaandering, R. Vidal, J. Whitmore, E. Wicklund, W. Wu, J. Yarba, F. Yumiceva, J.C. Yun

University of Florida, Gainesville, U.S.A.

D. Acosta, P. Avery, V. Barashko, D. Bourilkov, M. Chen, G.P. Di Giovanni, D. Dobur, A. Drozdetskiy, R.D. Field, Y. Fu, I.K. Furic, J. Gartner, D. Holmes, B. Kim, S. Klimenko, J. Konigsberg, A. Korytov, K. Kotov, A. Kropivnitskaya, T. Kypreos, A. Madorsky, K. Matchev, G. Mitselmakher, Y. Pakhotin, J. Piedra Gomez, C. Prescott, V. Rapsevicius, R. Remington, M. Schmitt, B. Scurlock, D. Wang, J. Yelton

Florida International University, Miami, U.S.A.

C. Ceron, V. Gaultney, L. Kramer, L.M. Lebolo, S. Linn, P. Markowitz, G. Martinez, J.L. Rodriguez

Florida State University, Tallahassee, U.S.A.

T. Adams, A. Askew, H. Baer, M. Bertoldi, J. Chen, W.G.D. Dharmaratna, S.V. Gleyzer, J. Haas, S. Hagopian, V. Hagopian, M. Jenkins, K.F. Johnson, E. Prettner, H. Prosper, S. Sekmen

Florida Institute of Technology, Melbourne, U.S.A.

M.M. Baarmand, S. Guragain, M. Hohlmann, H. Kalakhety, H. Mermerkaya, R. Ralich, I. Vodopyanov

University of Illinois at Chicago (UIC), Chicago, U.S.A.

B. Abelev, M.R. Adams, I.M. Anghel, L. Apanasevich, V.E. Bazterra, R.R. Betts, J. Callner, M.A. Castro, R. Cavanaugh, C. Dragoiu, E.J. Garcia-Solis, C.E. Gerber, D.J. Hofman, S. Khalatian, C. Mironov, E. Shabalina, A. Smoron, N. Varelas

The University of Iowa, Iowa City, U.S.A.

U. Akgun, E.A. Albayrak, A.S. Ayan, B. Bilki, R. Briggs, K. Cankocak³⁶, K. Chung, W. Clarida, P. Debbins, F. Duru, F.D. Ingram, C.K. Lae, E. McCliment, J.-P. Merlo, A. Mestvirishvili, M.J. Miller, A. Moeller, J. Nachtman, C.R. Newsom, E. Norbeck, J. Olson, Y. Onel, F. Ozok, J. Parsons, I. Schmidt, S. Sen, J. Wetzell, T. Yetkin, K. Yi

Johns Hopkins University, Baltimore, U.S.A.

B.A. Barnett, B. Blumenfeld, A. Bonato, C.Y. Chien, D. Fehling, G. Giurgiu, A.V. Gritsan, Z.J. Guo, P. Maksimovic, S. Rappoccio, M. Swartz, N.V. Tran, Y. Zhang

The University of Kansas, Lawrence, U.S.A.

P. Baringer, A. Bean, O. Grachov, M. Murray, V. Radicci, S. Sanders, J.S. Wood, V. Zhukova

Kansas State University, Manhattan, U.S.A.

D. Bandurin, T. Bolton, K. Kaadze, A. Liu, Y. Maravin, D. Onoprienko, I. Svintradze, Z. Wan

Lawrence Livermore National Laboratory, Livermore, U.S.A.

J. Gronberg, J. Hollar, D. Lange, D. Wright

University of Maryland, College Park, U.S.A.

D. Baden, R. Bard, M. Boutemour, S.C. Eno, D. Ferencek, N.J. Hadley, R.G. Kellogg, M. Kirn, S. Kunori, K. Rossato, P. Rumerio, F. Santanastasio, A. Skuja, J. Temple, M.B. Tonjes, S.C. Tonwar, T. Toole, E. Twedt

Massachusetts Institute of Technology, Cambridge, U.S.A.

B. Alver, G. Bauer, J. Bendavid, W. Busza, E. Butz, I.A. Cali, M. Chan, D. D'Enterria, P. Everaerts, G. Gomez Ceballos, K.A. Hahn, P. Harris, S. Jaditz, Y. Kim, M. Klute, Y.-J. Lee, W. Li, C. Loizides, T. Ma, M. Miller, S. Nahn, C. Paus, C. Roland, G. Roland, M. Rudolph, G. Stephans, K. Sumorok, K. Sung, S. Vaurynovich, E.A. Wenger, B. Wyslouch, S. Xie, Y. Yilmaz, A.S. Yoon

University of Minnesota, Minneapolis, U.S.A.

D. Bailleux, S.I. Cooper, P. Cushman, B. Dahmes, A. De Benedetti, A. Dolgoplov, P.R. Duderod, R. Egeland, G. Franzoni, J. Haupt, A. Inyakin³⁷, K. Klapoetke, Y. Kubota, J. Mans, N. Mirman, D. Petyt, V. Rekovic, R. Rusack, M. Schroeder, A. Singovsky, J. Zhang

University of Mississippi, University, U.S.A.

L.M. Cremaldi, R. Godang, R. Kroeger, L. Perera, R. Rahmat, D.A. Sanders, P. Sonnek, D. Summers

University of Nebraska-Lincoln, Lincoln, U.S.A.

K. Bloom, B. Bockelman, S. Bose, J. Butt, D.R. Claes, A. Dominguez, M. Eads, J. Keller, T. Kelly, I. Kravchenko, J. Lazo-Flores, C. Lundstedt, H. Malbouisson, S. Malik, G.R. Snow

State University of New York at Buffalo, Buffalo, U.S.A.

U. Baur, I. Iashvili, A. Kharchilava, A. Kumar, K. Smith, M. Strang

Northeastern University, Boston, U.S.A.

G. Alverson, E. Barberis, O. Boeriu, G. Eulisse, G. Govi, T. McCauley, Y. Musienko³⁸, S. Muzaffar, I. Osborne, T. Paul, S. Reucroft, J. Swain, L. Taylor, L. Tuura

Northwestern University, Evanston, U.S.A.

A. Anastassov, B. Gobbi, A. Kubik, R.A. Ofierzynski, A. Pozdnyakov, M. Schmitt, S. Stoynev, M. Velasco, S. Won

University of Notre Dame, Notre Dame, U.S.A.

L. Antonelli, D. Berry, M. Hildreth, C. Jessop, D.J. Karmgard, T. Kolberg, K. Lannon, S. Lynch, N. Marinelli, D.M. Morse, R. Ruchti, J. Slaunwhite, J. Warchol, M. Wayne

The Ohio State University, Columbus, U.S.A.

B. Bylsma, L.S. Durkin, J. Gilmore³⁹, J. Gu, P. Killewald, T.Y. Ling, G. Williams

Princeton University, Princeton, U.S.A.

N. Adam, E. Berry, P. Elmer, A. Garmash, D. Gerbaudo, V. Halyo, A. Hunt, J. Jones, E. Laird, D. Marlow, T. Medvedeva, M. Mooney, J. Olsen, P. Piroué, D. Stickland, C. Tully, J.S. Werner, T. Wildish, Z. Xie, A. Zuranski

University of Puerto Rico, Mayaguez, U.S.A.

J.G. Acosta, M. Bonnett Del Alamo, X.T. Huang, A. Lopez, H. Mendez, S. Oliveros, J.E. Ramirez Vargas, N. Santacruz, A. Zatzerklyany

Purdue University, West Lafayette, U.S.A.

E. Alagoz, E. Antillon, V.E. Barnes, G. Bolla, D. Bortoletto, A. Everett, A.F. Garfinkel, Z. Gecse, L. Gutay, N. Ippolito, M. Jones, O. Koybasi, A.T. Laasanen, N. Leonardo, C. Liu, V. Maroussov, P. Merkel, D.H. Miller, N. Neumeister, A. Sedov, I. Shipsey, H.D. Yoo, Y. Zheng

Purdue University Calumet, Hammond, U.S.A.

P. Jindal, N. Parashar

Rice University, Houston, U.S.A.

V. Cuplov, K.M. Ecklund, F.J.M. Geurts, J.H. Liu, D. Maronde, M. Matveev, B.P. Padley, R. Redjimi, J. Roberts, L. Sabbatini, A. Tumanov

University of Rochester, Rochester, U.S.A.

B. Betchart, A. Bodek, H. Budd, Y.S. Chung, P. de Barbaro, R. Demina, H. Flacher, Y. Gotra, A. Harel, S. Korjenevski, D.C. Miner, D. Orbaker, G. Petrillo, D. Vishnevskiy, M. Zielinski

The Rockefeller University, New York, U.S.A.

A. Bhatti, L. Demortier, K. Goulios, K. Hatakeyama, G. Lungu, C. Mesropian, M. Yan

Rutgers, the State University of New Jersey, Piscataway, U.S.A.

O. Atramentov, E. Bartz, Y. Gershtein, E. Halkiadakis, D. Hits, A. Lath, K. Rose, S. Schnetzer, S. Somalwar, R. Stone, S. Thomas, T.L. Watts

University of Tennessee, Knoxville, U.S.A.

G. Cerizza, M. Hollingsworth, S. Spanier, Z.C. Yang, A. York

Texas A&M University, College Station, U.S.A.

J. Asaadi, A. Aurisano, R. Eusebi, A. Golyash, A. Gurrola, T. Kamon, C.N. Nguyen, J. Pivarski, A. Safonov, S. Sengupta, D. Toback, M. Weinberger

Texas Tech University, Lubbock, U.S.A.

N. Akchurin, L. Berntzon, K. Gumus, C. Jeong, H. Kim, S.W. Lee, S. Popescu, Y. Roh, A. Sill, I. Volobouev, E. Washington, R. Wigmans, E. Yazgan

Vanderbilt University, Nashville, U.S.A.

D. Engh, C. Florez, W. Johns, S. Pathak, P. Sheldon

University of Virginia, Charlottesville, U.S.A.

D. Andelin, M.W. Arenton, M. Balazs, S. Boutle, M. Buehler, S. Conetti, B. Cox, R. Hirosky, A. Ledovskoy, C. Neu, D. Phillips II, M. Ronquest, R. Yohay

Wayne State University, Detroit, U.S.A.

S. Gollapinni, K. Gunthoti, R. Harr, P.E. Karchin, M. Mattson, A. Sakharov

University of Wisconsin, Madison, U.S.A.

M. Anderson, M. Bachtis, J.N. Bellinger, D. Carlsmith, I. Crotty¹, S. Dasu, S. Dutta, J. Efron, F. Feyzi, K. Flood, L. Gray, K.S. Grogg, M. Grothe, R. Hall-Wilton¹, M. Jaworski, P. Klabbers, J. Klukas, A. Lanaro, C. Lazaridis, J. Leonard, R. Loveless, M. Magrans de Abril, A. Mohapatra, G. Ott, G. Polese, D. Reeder, A. Savin, W.H. Smith, A. Sourkov⁴⁰, J. Swanson, M. Weinberg, D. Wenman, M. Wensveen, A. White

†: Deceased

- 1: Also at CERN, European Organization for Nuclear Research, Geneva, Switzerland
- 2: Also at Universidade Federal do ABC, Santo Andre, Brazil
- 3: Also at Soltan Institute for Nuclear Studies, Warsaw, Poland
- 4: Also at Université de Haute-Alsace, Mulhouse, France
- 5: Also at Centre de Calcul de l'Institut National de Physique Nucleaire et de Physique des Particules (IN2P3), Villeurbanne, France
- 6: Also at Moscow State University, Moscow, Russia
- 7: Also at Institute of Nuclear Research ATOMKI, Debrecen, Hungary
- 8: Also at University of California, San Diego, La Jolla, U.S.A.
- 9: Also at Tata Institute of Fundamental Research - HECR, Mumbai, India
- 10: Also at University of Visva-Bharati, Santiniketan, India
- 11: Also at Facolta' Ingegneria Universita' di Roma "La Sapienza", Roma, Italy
- 12: Also at Università della Basilicata, Potenza, Italy
- 13: Also at Laboratori Nazionali di Legnaro dell' INFN, Legnaro, Italy
- 14: Also at Università di Trento, Trento, Italy
- 15: Also at ENEA - Casaccia Research Center, S. Maria di Galeria, Italy
- 16: Also at Warsaw University of Technology, Institute of Electronic Systems, Warsaw, Poland
- 17: Also at California Institute of Technology, Pasadena, U.S.A.
- 18: Also at Faculty of Physics of University of Belgrade, Belgrade, Serbia
- 19: Also at Laboratoire Leprince-Ringuet, Ecole Polytechnique, IN2P3-CNRS, Palaiseau, France
- 20: Also at Alstom Contracting, Geneve, Switzerland
- 21: Also at Scuola Normale e Sezione dell' INFN, Pisa, Italy
- 22: Also at University of Athens, Athens, Greece
- 23: Also at The University of Kansas, Lawrence, U.S.A.
- 24: Also at Institute for Theoretical and Experimental Physics, Moscow, Russia
- 25: Also at Paul Scherrer Institut, Villigen, Switzerland
- 26: Also at Vinca Institute of Nuclear Sciences, Belgrade, Serbia
- 27: Also at University of Wisconsin, Madison, U.S.A.
- 28: Also at Mersin University, Mersin, Turkey
- 29: Also at Izmir Institute of Technology, Izmir, Turkey
- 30: Also at Kafkas University, Kars, Turkey
- 31: Also at Suleyman Demirel University, Isparta, Turkey
- 32: Also at Ege University, Izmir, Turkey

- 33: Also at Rutherford Appleton Laboratory, Didcot, United Kingdom
- 34: Also at INFN Sezione di Perugia; Universita di Perugia, Perugia, Italy
- 35: Also at KFKI Research Institute for Particle and Nuclear Physics, Budapest, Hungary
- 36: Also at Istanbul Technical University, Istanbul, Turkey
- 37: Also at University of Minnesota, Minneapolis, U.S.A.
- 38: Also at Institute for Nuclear Research, Moscow, Russia
- 39: Also at Texas A&M University, College Station, U.S.A.
- 40: Also at State Research Center of Russian Federation, Institute for High Energy Physics, Protvino, Russia